Global Biogeochemical Cycles

RESEARCH ARTICLE
10.1029/2023GB007756

Key Points:

- Simulated *Prochlorococcus*, *Synechococcus*, and pico-eukaryotes contribute ~60% of marine net primary productivity (NPP)
- Pico-phytoplankton cycling contributes half of the marine export production, approaching parity with their contribution to NPP
- Pico-eukaryotes and diatoms with elevated C:P stoichiometry enhance carbon export at poleward flanks of western boundary currents

Correspondence to:
R. T. Letscher,
robert.letscher@unh.edu

Citation:
Letscher, R. T., Moore, J. K., Martiny, A. C., & Lomas, M. W. (2023). Biodiversity and stoichiometric plasticity increase pico-phytoplankton contributions to marine net primary productivity and the biological pump. *Global Biogeochemical Cycles*, *37*, e2023GB007756. https://doi.org/10.1029/2023GB007756

Received 27 FEB 2023
Accepted 27 JUL 2023

Author Contributions:
Conceptualization: Robert T. Letscher, J. Keith Moore, Adam C. Martiny
Data curation: Michael W. Lomas
Formal analysis: Robert T. Letscher, J. Keith Moore
Funding acquisition: Robert T. Letscher, J. Keith Moore
Methodology: Robert T. Letscher, J. Keith Moore
Project Administration: J. Keith Moore
Resources: Michael W. Lomas
Software: Robert T. Letscher, J. Keith Moore
Validation: Robert T. Letscher, J. Keith Moore, Adam C. Martiny, Michael W. Lomas
Visualization: Robert T. Letscher
Writing – original draft: Robert T. Letscher
Writing – review & editing: Robert T. Letscher, J. Keith Moore, Adam C. Martiny, Michael W. Lomas

Biodiversity and Stoichiometric Plasticity Increase Pico-Phytoplankton Contributions to Marine Net Primary Productivity and the Biological Pump

Robert T. Letscher[1,2], J. Keith Moore[3], Adam C. Martiny[3,4], and Michael W. Lomas[5]

[1]Ocean Process Analysis Laboratory, University of New Hampshire, Durham, NH, USA, [2]Earth Sciences, University of New Hampshire, Durham, NH, USA, [3]Earth System Science, University of California, Irvine, CA, USA, [4]Ecology and Evolutionary Biology, University of California, Irvine, CA, USA, [5]Bigelow Laboratory for Ocean Sciences, East Boothbay, ME, USA

Abstract Earth System Models generally predict increasing upper ocean stratification from 21st century warming, which will cause a decrease in the vertical nutrient flux forcing declines in marine net primary productivity (NPP) and carbon export. Recent advances in quantifying marine ecosystem carbon to nutrient stoichiometry have identified large latitudinal and biome variability, with low-latitude oligotrophic systems harboring pico-sized phytoplankton exhibiting large phosphorus to carbon cellular plasticity. The climate forced changes in nutrient flux stoichiometry and phytoplankton community composition are thus likely to alter the ocean's biogeochemical response and feedback with the carbon-climate system. We have added three pico-phytoplankton functional types within the Biogeochemical Elemental Cycling component of the Community Earth System Model while incorporating variable cellular phosphorus to carbon stoichiometry for all represented phytoplankton types. The model simulates *Prochlorococcus* and *Synechococcus* populations that dominate the productivity and sinking carbon export of the tropical and subtropical ocean, and pico-eukaryote populations that contribute significantly to productivity and export within the subtropical to mid-latitude transition zone, with the western subtropical regions of each basin supporting the most P-poor stoichiometries. Subtropical gyre recirculation regions along the poleward flanks of surface western boundary currents are identified as regional hotspots of enhanced carbon export exhibiting C-rich/P-poor stoichiometry, preferentially inhabited by pico-eukaryotes and diatoms. Collectively, pico-phytoplankton contribute ~58% of global NPP and ~46% of global particulate organic carbon export below 100 m through direct and ecosystem processing pathways. Biodiversity and cellular nutrient plasticity in marine pico-phytoplankton combine to increase their contributions to ocean productivity and the biological carbon pump.

1. Introduction

Ocean biogeochemical (OBGC) models operating within larger Earth System Models (ESMs) have been developed to quantify feedbacks between ocean biology, chemistry, and the climate system and project ocean biogeochemistry fluxes and tracer concentrations decades to centuries into the future (Bopp et al., 2013; Cabré et al., 2015; Friedlingstein et al., 2006; Moore et al., 2013, 2018; Quéré et al., 2005). ESM output from the Coupled Model Intercomparison Project Phase 5 (CMIP5) and Phase 6 (CMIP6) has projected ocean acidification, deoxygenation, and decreasing primary productivity during the 21st century (Bopp et al., 2013; Cabré et al., 2015; Kwiatkowski et al., 2020; Moore et al., 2013) and beyond (Moore et al., 2018) under a worse-case scenario, primarily as a result of changes in ocean circulation and stratification in response to warming ocean temperatures. Enhanced upper ocean stratification leads to a reduction in vertical nutrient flux to the sunlight surface layer of the low latitudes, decreasing net primary productivity (NPP) by phytoplankton, with a concomitant reduction in carbon export to the ocean interior (Cabré et al., 2015; Wilson et al., 2022), resulting in positive feedback with the climate system as ocean carbon uptake is diminished with sustained warming. These declines are nearly universal among CMIP5 models, most of which feature fixed C:N:P:$-O_2$ stoichiometry (i.e., the Redfield ratio; Redfield, 1934, 1958) to describe phytoplankton nutrient uptake, production of organic matter, and its subsequent remineralization (Bopp et al., 2013). Further, declines in key carbon cycle features persist in the latest generation CMIP6 models despite an increasingly prevalent switch to a variable nutrient to carbon quotas within the marine biogeochemistry modules (Séférian et al., 2020; Wilson et al., 2022).

Common to nearly all OBGC models is the representation of one or more "functional groups or types" of phytoplankton (Quéré et al., 2005) that consume inorganic nutrients, resulting in photosynthesis, net primary production, and production of autotrophic biomass. Autotrophy is most often distributed among ≥2 phytoplankton functional types (PFTs), that are chosen to represent differing growth strategies, for example, slower-growing small pico- and nano-phytoplankton versus fast-growing large diatoms based on allometric theory (Moloney & Field, 1989), to capture biogeographic latitudinal trends in nutrient uptake rates, cell size, and export efficiency. Phytoplankton growth experiences top-down control due to grazing by one or more zooplankton groups, also resulting in the production of particulate and dissolved organic detrital pools. Bottom-up controls on phytoplankton growth include multiple nutrient limitations, light limitation, and optimum temperature effects. Generally, nutrient uptake affinity is inversely correlated with cell size, with smaller PFTs better able to acquire nutrients at low in situ concentrations. Each PFT acquires nutrients to satisfy their particular cellular N:C, P:C, and/or Fe:C quota, depending on the simulated inorganic nutrient fields. These cellular nutrient quotas are invariant for fixed stoichiometry models (i.e., at Redfield proportions; Aumont et al., 2015; Dunne et al., 2010; Ilyina et al., 2013; Moore et al., 2004) or can be variable, dependent on in situ environmental parameters such as nutrient concentration (Galbraith & Martiny, 2015) or optimal resource allocation theory describing phytoplankton cellular functions (Dunne, 2013; Klausmeier et al., 2004; Kwiatkowski et al., 2018). Many culture and field observations have documented variability in cellular nutrient quotas that vary both with ambient nutrient concentrations (Karl et al., 2001; Rhee, 1978; Tanioka et al., 2022) and/or across PFTs (Baer et al., 2017; Geider & La Roche, 2002; Martiny et al., 2013a; Quigg et al., 2003). Additionally, with the emergence of flow cytometry for the study of marine microbes (Lomas et al., 2011), a large literature of field and culture-based studies have accumulated in recent decades describing the physiology, biogeography, and phylogeny of marine pico-phytoplankton, more specifically the cyanobacterial lineages *Prochlorococcus* and *Synechococcus* and pico-eukaryotic phytoplankton, which now allows for their representation in numerical marine ecosystem models (e.g., Baer et al., 2017; Buitenhuis et al., 2012; DuRand et al., 2001; Flombaum et al., 2013, 2020; Martiny et al., 2009; Moore et al., 1998; Partensky et al., 1999; Pasulka et al., 2013; Sohm et al., 2016). Given the need to balance model complexity against limiting computational resources, the representation of additional pico-phytoplankton groups is perhaps of first order importance with respect to the introduction of variable elemental stoichiometry within OBGC models since pico-phytoplankton are known to exhibit the largest carbon to nutrient cellular plasticity (Baer et al., 2017; Martiny et al., 2013a; Quigg et al., 2003). In light of these advances, representing the pico-phytoplankton and variable carbon to nutrient content of all phytoplankton in OBGC models has become a pressing goal to better capture the ocean ecosystem response to the changing 21st century climate and its associated feedbacks with the climate system.

Many recent studies have identified and quantified the non-Redfield, variable carbon to nutrient stoichiometry that permeates most OBGC fluxes and tracer pools including dissolved nutrients (Weber & Deutsch, 2010), biomass (Tanioka & Matsumoto, 2020), particulate organic matter (Martiny et al., 2013a), Dissolved organic matter (DOM) (Letscher & Moore, 2015), export production (Teng et al., 2014), and organic matter remineralization (DeVries & Deutsch, 2014). The emergent pattern from these studies is one of carbon-rich (nutrient-poor) stoichiometry that describes biogeochemical functioning in the lower latitude, nutrient-poor biomes of the subtropics, while the nutrient-replete upwelling and subpolar biomes exhibit stoichiometries at or slightly below Redfield carbon to nutrient proportions. Two mechanisms have been suggested to contribute to the observed biogeography of marine ecosystem stoichiometry including phosphorus and/or nitrogen plasticity by the extant phytoplankton community (e.g., Galbraith & Martiny, 2015; Van Mooy et al., 2009) as well as shifts in phytoplankton community composition across biomes with relatively nutrient-deficient cyanobacteria dominating the subtropics and more nutrient-rich diatoms and other larger phytoplankton dominating elsewhere (e.g., Arrigo et al., 1999; Sharoni & Halevy, 2020; Weber & Deutsch, 2010). Cell-sorted field populations of cyanobacteria (*Prochlorococcus* and *Synechococcus*) and pico-eukaryotes from the Sargasso Sea, eastern Pacific, and the Indian Ocean suggest both mechanisms may be at play as cyanobacteria exhibited lower cellular P content as compared to eukaryotes, while all groups exhibited cellular P plasticity in response to latitudinal gradients in inorganic phosphorus availability, albeit at varying degrees across taxonomic groups (Baer et al., 2017; Lomas et al., 2021; Martiny et al., 2013a).

Does representation of variable carbon to nutrient stoichiometry within OBGC models potentially buffer the well-documented positive ocean carbon cycle feedback to future climate warming? A number of ESM's that have included representation of variable carbon to phosphorus stoichiometry within the ocean ecosystem

component generally predict a more resilient response for future marine NPP and carbon export fluxes, with modest ~0 – <5% declines by year 2100 (Buchanan et al., 2018; Kwiatkowski et al., 2018; Kwon et al., 2022; Matsumoto et al., 2020; Tanioka & Matsumoto, 2017). The inclusion of variable phosphorus to carbon stoichiometry within the marine ecosystem component permits flexibility in phytoplankton phosphorus quotas. Such frugal use of nutrients allows phytoplankton to maintain similar growth rates under decreasing P flux as well as a shift towards increasing biomass C:P that partially compensates for warming induced changes to ocean circulation and stratification. Galbraith and Martiny (2015) demonstrated with a simple box model that changes to the preformed phosphate concentration on the order of 100 nM within low latitude surface waters can produce up to 20 ppm shifts in atmospheric CO_2 concentrations, assuming P is the primary growth limiting nutrient. An OBGC modeling study incorporating representation of variable marine elemental stoichiometry found that adding this sensitivity buffered against a predicted decrease in global carbon export production of the order of ~3% for the 21st century (Tanioka & Matsumoto, 2017). Similarly, results from the recent inclusion of this process within the Pelagic Interactions Scheme for Carbon and Ecosystem Studies Quota (PISCES-QUOTA) model suggest its effects on 21st century ocean carbon uptake are modest with up to a 3.5% underestimation as compared to fixed stoichiometry ESMs (Kwiatkowski et al., 2018). However, larger regional changes of up to 50% reductions or stimulations of marine NPP and carbon export were predicted which could have significant local to regional impacts on marine ecosystems and fisheries. The above studies have thus far considered adaptive nutrient quotas, while other phytoplankton adaptive strategies including altered physiological rates, trait-based evolution, and changes in grazing pressure could all potentially influence phytoplankton fitness and resilience with important controls on marine NPP and carbon export trends (Martiny et al., 2022).

As the next generation of OBGC models mature to better represent variable carbon to nutrient stoichiometry with the goal to study how this variability impacts the marine NPP and carbon export fluxes, an important missing element to this question is the role for changes in marine phytoplankton biodiversity to modulate the response. Most of the current generation of OBGC models represent the marine phytoplankton community with 1–3 PFTs, with the notable exception of the ECCO-Darwin OBGC model, which simulates 35 to 350 PFTs (e.g., Dutkiewicz et al., 2020; Juranek et al., 2020). This higher biodiversity model has been shown to more accurately represent the marine phytoplankton diversity regionally to globally, as gauged by metrics such as phytoplankton size distribution, biomass, size-fractionated NPP rates, and species richness. How do marine phytoplankton diversity and associated carbon to nutrient stoichiometric variability impact the regional to global patterns of carbon export? Based on current understanding, enhanced thermal stratification of the water column depresses the vertical nutrient input, favoring a shift to smaller sized pico-phytoplankton dominated by cyanobacteria possessing higher plasticity in cellular nutrient quotas. Thus, in a future warmer ocean with expanding stratification, the marine biodiversity response might be hypothesized to favor marine cyanobacteria such as *Prochlorococcus*, *Synechococcus*, and the marine N_2-fixing *Trichodesmium* (Hutchins et al., 2007) with elevated C:P cellular stoichiometry. While the shift to smaller phytoplankton may depress marine NPP rates, export of a portion of the resultant biomass with high C:P may partially buffer against reductions in marine carbon export and mitigate the expected positive feedback to warming by maintaining the strength of the ocean's biological carbon pump. In support of this hypothesis, observations from the Bermuda Atlantic Time-series station in the Sargasso Sea document a recent decline in marine NPP due to enhanced stratification, without a concomitant decline in carbon export, explained by a shift in the phytoplankton community composition in favor of cyanobacteria with higher cellular C:P stoichiometry (Lomas et al., 2022). Additionally, high latitudes systems such as the Southern Ocean might respond differently to enhanced stratification, increasing biological productivity and associated carbon export (Bopp et al., 2013), potentially contributing an additional buffer against biological carbon pump reductions in a warming ocean.

This paper describes the addition of three new pico-phytoplankton functional types, *Prochlorococcus*, *Synechococcus*, and pico-eukaryotes, to the OBGC component of the Community Earth System Model (CESM), with the goal to better characterize the role for marine phytoplankton biodiversity and associated variable cellular carbon to phosphorus stoichiometry in controlling marine carbon export patterns. The implementation builds from recent advances in this OBGC model to incorporate variable C:P stoichiometry within all pertinent tracers of the marine ecosystem (Letscher et al., 2015; Wang et al., 2019) including phytoplankton, DOM, and sinking particulate organic matter, to now include a representation of six PFTs: *Prochlorococcus*, *Synechococcus*, pico-eukaryotes, nano-phytoplankton (including implicit coccolithophores), diatoms, and diazotrophs.

2. Methods

The model is the Biogeochemical Elemental Cycling (BEC), which is the biogeochemistry and ecosystem component operating within the ocean circulation model (Parallel Ocean Program 2 (POP2)) of the CESM v.1.2.2 (http://www.cesm.ucar.edu/models/cesm1.2/). The model resolution employed here is nominally 3° × 3° horizontally with 60 vertical layers (gx3v7 grid) that increase in thickness with depth in the water column. The ocean circulation is the output of the POP2 ocean circulation model using the final 30-year forcing from years 1980–2009 of the Coordinated Ocean-ice Reference Experiments-Phase II (CORE-II) forcing (Smith et al., 2010) and includes parameter value changes to the isopycnal diffusivity (κ_{isop}) to partially account for the transport of unresolved equatorial jets (Getzlaff & Dietze, 2013).

The BEC tracks the cycling of key biogeochemical tracers (e.g., C, N, P, Fe, and O_2) among dissolved inorganic, dissolved organic, sinking particulate, and four plankton biomass pools (Moore et al., 2004). Net primary production in the model is partitioned amongst three PFTs–small phytoplankton (with implicit calcifiers), diatoms, and diazotrophs, which differ in their relative competitiveness for limiting nutrients (N, P, Si, and Fe). In addition to bottom-up nutrient and light control, phytoplankton mortality is controlled top-down by grazing from one zooplankton group. Version 1.2.2 of the BEC contains significant improvements to the cycling of marine DOM (Letscher et al., 2015). A more recent model development for BEC v1.2.2 has incorporated variable phosphorus quotas for the three phytoplankton types (Wang et al., 2019) that depend on in situ simulated inorganic phosphate concentration following the linear relationship in Galbraith and Martiny (2015) but with imposed minimum (110:1) and maximum (210:1) C:P values for all PFTs. This current work describes the addition of three new pico-phytoplankton groups with variable carbon to nutrient (P and Fe) stoichiometry to the BEC model, building from the code base for the variable 3 PFT phosphorus quota model of Wang et al. (2019). The "small phytoplankton" group from the 3 PFT BEC model, which jointly represented pico- and nano-sized phytoplankton, has been reparameterized to more closely represent larger nano-phytoplankton. The newly named nano-phytoplankton along with the diatom and diazotroph groups are updated to represent variable C:P and C:Fe stoichiometry. The model retains one zooplankton group with Redfieldian stoichiometry. The marine ecosystem in the BEC model is thus represented by 6 phytoplankton and 1 zooplankton groups, or 6p1z.

The addition of three pico-phytoplankton groups with variable carbon to nutrient stoichiometry introduces 12 additional tracers to the BEC model code: biomass carbon (C), chlorophyll (Chl), iron (Fe), and phosphorus (P) for each of the 3 pico-phytoplankton groups, termed "Prochlorococcus" (pro), "*Synechococcus*" (syn), and "Pico-eukaryotes" (peuk). The "small phytoplankton" group from BEC v1.2.2 and earlier versions has been renamed "nano-phytoplankton" (nano) and retains the implicit calcifiers. Nano-phytoplankton as well as the diatoms (diat) and diazotroph (diaz) phytoplankton groups carry the same four biomass tracers (C, Chl, Fe, P) as the newly added pico-phytoplankton, with the addition of biomass silicon for diatoms. Variable biomass nitrogen (N) content is not considered at this time and phytoplankton biomass N:C is fixed for all six phytoplankton groups at a value of 0.1333 (C:N = 7.5) near the mean of open ocean suspended particles (Martiny et al., 2013b) and nutrient replete versus deplete cells across a range of phyla (Geider & La Roche, 2002).

Growth and mortality of each phytoplankton type is modeled with more than two dozen parameter values specific to each group, including half saturation constants for nutrient uptake, photosynthesis versus irradiance curves, Fe and P quotas, temperature thresholds for growth, contributions to detrital pools, and zooplankton grazing rates among others. Table 1 lists these parameter values for each phytoplankton group including the relevant literature sources. Where literature sources are insufficient to inform the value for a particular parameter, the principle of allometric scaling is employed to assign values corresponding with cell size to the order of increasing cell size as follows: pro/syn/peuk < nano/diaz < diat (Edwards et al., 2012; Flynn et al., 2018; Hein et al., 1995).

Phytoplankton iron uptake half saturation constants are prescribed with cyanobacteria having the lowest values (pro = 30 pM; syn + diaz = 40 pM), followed by pico-eukaryotes (43 pM), nano-eukaryotes (55 pM), and the large celled diatoms (60 pM) following the culture studies of Shire and Kustka (2015) and Timmermans et al. (2005) and the field study of Hutchins et al. (2002) (Table 1). Phosphate half saturation constants are selected based on the field study from the Sargasso Sea of Lomas et al. (2014), the culture study of N. S. Garcia et al. (2015), and the Amazon River plume ecosystem modeling work of Stukel et al. (2014) with kPO4 values increasing from a value of 8 nM for pro, 10 nM for syn, 15 nM for peuk, 25 nM for diaz, 40 nM for nano, and 70 nM for diatoms. Semilabile dissolved organic phosphorus (DOP) is bioavailable for phytoplankton to utilize

Global Biogeochemical Cycles

10.1029/2023GB007756

Table 1
Description of Phytoplankton Parameters and Values From the PICO Simulation of the Biogeochemical Elemental Cycling Model

Parameter	Description	Units	Pro	Syn	Peuk	Nano	Diat	Diaz	Reference
kFe	Half sat. const. diss. iron	mmol/m^3	0.030e−3	0.040e−3	0.043e−3	0.055e−3	0.06e−3	0.04e−3	Shire and Kustka (2015), Timmermans et al. (2005), and Hutchins et al. (2002)
kPO4	Half sat. const. phosphate	mmol/m^3	0.008	0.01	0.015	0.04	0.07	0.025	Lomas et al. (2014), Stukel et al. (2014), and N. S. Garcia et al. (2015)
kDOP	Half sat. const. diss. organic P	mmol/m^3	0.8	0.9	0.15	0.2	0.1	0.25	Casey et al. (2009), Orchard et al. (2010), Sohm and Capone (2006), and Dyhrman and Ruttenberg (2006)
kNO3	Half sat. const. nitrate	mmol/m^3	0.3	0.18	0.15	0.25	0.35	4.0	Hein et al. (1995), Edwards et al. (2012), and Flynn et al. (2018)
kNH4	Half sat. const. ammonium	mmol/m^3	0.005	0.008	0.011	0.02	0.035	0.4	Hein et al. (1995), Edwards et al. (2012), and Flynn et al. (2018)
gQfe_0	Initial Fe:C	Ratio	80e−6	80e−6	90e−6	90e−6	90e−6	180e−6	Boyd et al. (2015)
gQfe_min	Minimum Fe:C	Ratio	10.0e−6	10.0e−6	3.0e−6	3.0e−6	3.0e−6	6.0e−6	Boyd et al. (2015)
FeOpt	Threshold for reducing Fe quota	mmol/m^3	0.8e−3	0.8e−3	1.0e−3	1.6e−3	1.75e−3	1.5e−3	Boyd et al. (2015)
gQp_0	Initial P:C	Ratio	1.042e−2	1.042e−2	1.111e−2	1.111e−2	1.111e−2	6.667e−3	Galbraith and Martiny (2015) and Martiny et al. (2013a, 2013b)
gQp_min	Minimum P:C	Ratio	3.704e−3	5.208e−3	8.333e−3	8.333e−3	8.333e−3	3.333e−3	Galbraith and Martiny (2015) and Martiny et al. (2013a, 2013b)
POpt	Threshold for reducing P quota	mmol/m^3	0.5	0.5	0.75	1.0	1.0	0.5	Galbraith and Martiny (2015) and Martiny et al. (2013a, 2013b)
	Resulting max C:P	Ratio	270	192	120	120	120	300	
	Resulting max N:P	Ratio	45	32	20	20	20	50	
alphaPI	Initial slope of Photo-Irr curve	mmolC m^2/ mgChl W s	1.00	1.09	0.7	0.83	0.88	0.2	Stawiarski et al. (2018)
PCref	Maximum C-spec. growth rate	d^{-1}	3.6	3.6	3.8	3.8	4.0	1.9	Stawiarski et al. (2018)
thetaN_max	Maximum Chl:N	Ratio	3.33	2.20	3.55	3.00	4.00	2.00	Stawiarski et al. (2018)
loss_thres	Biomass where losses go to 0	mmolC/m^3	0.02	0.02	0.02	0.025	0.025	0.02	
temp_thres	Temp. where Photo rates drop	°C	13.0	4.0	−1.5	−10.0	−10.0	18.0	Flombaum et al. (2013, 2020)
mort	Mortality rate	d^{-1}	0.1	0.1	0.1	0.1	0.1	0.1	
agg_rate_max	Maximum aggregation rate	d^{-1}	0.5	0.5	0.5	0.5	0.8	0.5	
agg_rate_min	Minimum aggregation rate	d^{-1}	0.005	0.005	0.01	0.01	0.015	0.005	
z_umax_0	Maximum zoopl. growth rate	d^{-1}	2.66	2.60	2.97	2.80	2.70	2.80	
z_grz	Grazing coefficient	mmolC/m^3	1.3	1.6	1.95	1.8	1.58	1.3	

Table 1
Continued

Parameter	Description	Units	Pro	Syn	Peuk	Nano	Diat	Diaz	Reference
graze_zoo	Routing of grazing to zoopl.	Fraction	0.3	0.3	0.3	0.3	0.3	0.3	Lomas and Moran (2011)
graze_poc	Routing of grazing to POC	Fraction	0.07	0.09	0.13	0.28	0.40	0.03	
graze_doc	Routing of grazing to DOC	Fraction	0.06	0.06	0.06	0.06	0.06	0.06	Letscher et al. (2015)
f_zoo_detr	Fract. zoopl. losses to detrital	Fraction	0.33	0.32	0.3	0.2	0.2	0.36	

as a P source when phosphate levels are low in the BEC model (Letscher et al., 2015) with the half saturation constants for its uptake selected based on several field studies from the Sargasso Sea and eastern North Pacific (Casey et al., 2009; Dyhrman & Ruttenberg, 2006; Orchard et al., 2010; Sohm & Capone, 2006). Following these studies, eukaryotes and diazotrophs are assigned the lowest half saturation values for DOP uptake ranging from 100–250 nM, with higher kDOP values ranging from 800–900 nM for the two cyanobacteria groups. Half saturation constants for ammonium are assigned following allometric scaling in the range 5–35 nM. Nitrate uptake half saturation constants are similarly assigned following allometric scaling in the range 150–350 nM, with exceptions to syn and peuk which are assigned the lowest values of 180 and 150 nM respectively, owing to their demonstrated increased affinity for nitrate relative to pro in the Sargasso Sea (e.g., Fawcett et al., 2011; Glover et al., 1988) and observed correlations between peuk abundance and in situ nitrate (Flombaum et al., 2020). Diazotroph kNH4 and kNO3 are set to the highest value across the 6 PFTs to reflect its reliance on internally fixed N for a significant but not exclusive fraction of its N quota (Knapp, 2012).

Phytoplankton iron quotas in the BEC model allow for flexibility in phytoplankton biomass Fe:C based on in situ dissolved iron concentrations varying in the range of 3–180 μmol:mol (Table 1). Following the field study of Boyd et al. (2015), eukaryotes are assigned the lowest minimum iron quotas, followed by diazotrophs and non-N-fixing cyanobacteria (*Prochlorococcus* and *Synechococcus*). The diazotroph group is assigned the highest maximum iron quotas based on the high iron requirement of the nitrogen-fixing enzyme nitrogenase (Berman-Frank et al., 2007). Phytoplankton iron quotas are reduced linearly when in situ dissolved Fe concentrations fall below a prescribed threshold (FeOpt), set to 1.75 nM for diatoms, 1.6 nM for nano, 1.5 nM for diaz, 1.0 nM for peuk, and 0.8 nM for pro and syn (Wiseman et al., 2023).

Variable phosphorus quotas are implemented here for the six phytoplankton group BEC models following the approach introduced in Wang et al. (2019) and similar to the variable Fe:C approach described above. Variable phytoplankton biomass P:C is modeled as a function of in situ dissolved phosphate concentration using the linear relation detailed in Galbraith and Martiny (2015) diagnosed from a global compilation of suspended particulate organic phosphorus and carbon concentrations. Each PFT P:C quota (gQp) is computed using the below equation:

$$\begin{aligned} \mathrm{gQp} &= \left[\left(\frac{\mathrm{gQp\_0} - \mathrm{gQp\_min}}{\mathrm{POpt}}\right) \times \mathrm{PO4}\right] + \mathrm{gQp\_min} && \mathrm{PO4} < \mathrm{POpt} \\ \mathrm{gQp} &= \mathrm{gQp\_0} && \mathrm{PO4} \geq \mathrm{POpt} \end{aligned} \quad (1)$$

where PO4 is the in situ dissolved inorganic phosphate concentration (μM) and gQp_0 and gQp_min describe the maximum and minimum P:C quota (see Table 1). Equation 1 linearly decreases the phytoplankton P:C quota (increases its C:P ratio) below a prescribed threshold (POpt; range 0.5–1.0 μM across PFTs), from its initial maximum value, currently prescribed at gQp_0 = 0.01111; C:P = 90:1 for the eukaryotes (peuk + nano + diat), gQp_0 = 0.01042; C:P = 96:1 for the cyanobacteria, and gQp_0 = 0.006667; C:P = 150:1 for diazotrophs, toward a minimum P:C quota that varies for each PFT (Table 1). This formulation is similar in approach to that presented in Galbraith and Martiny (2015), in which field observations of the surface ocean particulate organic phosphorus to particulate organic carbon ratio (of which autotrophic biomass is a significant contributor) were found to fit a linear function of in situ dissolved phosphate concentration. The formulation presented here prescribes differing P:C versus PO4 slopes and y-intercepts for each PFT set by the choice of gQp_min. Field-based estimates of cell-sorted biomass C:P and N:P for *Prochlorococcus*, *Synechococcus*, and pico-eukaryotes from the Sargasso Sea (Martiny et al., 2013a) and elsewhere (Baer et al., 2017; Lomas et al., 2021) are used to assign values of gQp_min with a maximum C:P of 300:1 for diazotrophs, a C:P of 270:1 for *Prochlorococcus* and 192:1 for *Synechococcus*, and a maximum C:P of 120:1 for peuk, nano, and diat (retained from the variable C:P BEC model; Wang et al., 2019).

Based on the phytoplankton niche modeling of Flombaum et al. (2013, 2020), each phytoplankton group in the BEC is assigned a temperature threshold below which photosynthesis rates and thus growth rates are depressed, with *Prochlorococcus* and diazotroph niches favoring warmer temperatures above 13 and 18°C, respectively. *Synechococcus* and pico-eukaryote growth decreases as temperatures fall below 4 and −1.5°C, respectively, while nano-phytoplankton and diatom growth rates are not depressed as a function of temperature (temp_thres value set to −10°C in Table 1).

Physiological response to light parameters describing the pico-phytoplankton are assigned based on the culture study of Stawiarski et al. (2018) in which two strains of *Prochlorococcus* (HL RCC 296, LL RCC 162), one *Synechococcus* strain (RCC 30), and four pico-eukaryote species *Triparma eleuthera* (RCC 212), *Micromonas pusilla* (RCC 1677), *Picochlorum* sp. (TCC 289), and *Nannochloropsis granulata* (RCC 438) from the Roscoff culture collection (Vaulot et al., 2004) were studied. Following this study, cyanobacteria are assigned slower maximum growth rates than eukaryotes, in the range 1.9–4 d^{-1} (based on a 24-hr light period). Stawiarski et al. (2108) found that light affinity is inversely related to the maximum growth rate. *Prochlorococcus* and *Synechococcus* are assigned the highest light affinities, as encoded within the "alphaPI" model parameter which describes the initial slope of the photosynthesis-irradiance curve, with decreasing affinities for the faster growing eukaryotes (Table 1). The maximum Chl:N, the "thetaN_max" model parameter, is assigned inversely proportional to the maximum growth rate with the exception of *Synechococcus*, which exhibits lower Chl:C in line with the results of Stawiarski et al. (2018).

Grazing on each of the six phytoplankton groups in the updated BEC model is carried out by one adaptive zooplankton group employing passive switching between phytoplankton prey. The grazing formulation follows a Holling Type II functional response as follows:

$$G(P_i) = {z_{0_i}}^{\max} * T_f * \left(\frac{P_i}{P_i + {K_i}^P}\right) * Z \tag{2}$$

where the grazing rate (G) on phytoplankton group i (Pi) is computed as a function of the maximum grazing rate (${z_{0i}}^{\max}$), the zooplankton biomass (Z), a saturation term (${P_i}/{P_i} + {K_i}^P$) where ${K_i}^P$ is half saturation constant, and $T_f = 1.7 \times \exp[(T - 30°C)/10°C]$, a temperature dependence term (Long et al., 2021). The maximum grazing rate, "z_umax_0" parameter, and grazing half saturation constant "z_grz" parameter in Table 1 vary depending on the autotroph type being consumed. The effective grazing rates are slower on larger phytoplankton and faster on smaller phytoplankton groups to reflect the differing predator-prey dynamics involving microzooplankton versus mesozooplankton (Moore et al., 2004). Grazing rates are largely unconstrained by field data. In the BEC model, maximum grazing rates are adjusted to achieve satisfactory biomass distributions and C:P stoichiometry for each phytoplankton group as validated against phytoplankton niche modeling and flow-sorted biomass stoichiometry distributions. Variable fractions of phytoplankton biomass are routed to zooplankton losses to detritus (e.g., fecal pellets) and particulate organic matter pools resulting from zooplankton grazing (Table 1). Each PFT's contribution to the sinking export flux following grazing varies from a minimum of 3% for diazotrophs to a maximum of 40% for diatoms ("graze_poc"; Table 1), informed in part by pigment biomarker analyses of the sediment trap flux in the Sargasso Sea (Lomas & Moran, 2011). Zooplankton contribute varying proportions of grazed phytoplankton biomass to detritus (POC) based on the PFT grazed, ranging from a minimum of 20% for nano-phytoplankton and diatoms to a maximum of 36% when grazing diazotrophs ("f_zoo_detr"; Table 1). Grazing of phytoplankton biomass also contributes 6% to the DOM pool following the inverse model-diagnosed rate from our previous work (Letscher et al., 2015).

BEC simulations were initially carried out for 60 model years from initial conditions, allowing the upper ocean ecosystem to achieve a quasi-equilibrium, <1% tracer concentration change per decade. After the selection of the set of parameter values that best matched observational constraints, a longer 300 model year simulation was performed, repeating the 30-year (1980–2009) CORE-II forcing for a total of 10 repetitions. The annually averaged output for the final 20 years of this simulation were averaged and is presented in all results to follow. Reported flux variability represents ±1 S.D. of the mean for the 20 years of output. The BEC simulation containing the additional pico-phytoplankton groups for a total of 6 PFTs is termed PICO. In Section 3, this simulation is compared against two similarly forced previous versions of the BEC model: a variable C:P stoichiometry version with 3 PFTs herein termed VAR-3 (Wang et al., 2019) and a 3 PFT version with Redfield stoichiometry governing phytoplankton dynamics herein termed RED-3 (Letscher et al., 2015).

The output of the PICO simulation is validated for the simulation of chlorophyll *a* and NPP against the Sea-Viewing Wide Field-of-View Sensor (SeaWiFS) satellite mission climatology products (1997–2010) related to chlorophyll *a* concentration (NASA GSFC, 2018) and a model of carbon-based NPP estimated from SeaWiFS data products (Behrenfeld et al., 2005; Westberry et al., 2008). Simulated nutrient concentrations from the pico-phytoplankton BEC model are compared with the World Ocean Atlas (WOA) 2013 climatologies of nitrate, phosphate, and silicate (H. E. Garcia et al., 2013) and a global compilation of dissolved Fe concentrations (Tagliabue et al., 2012).

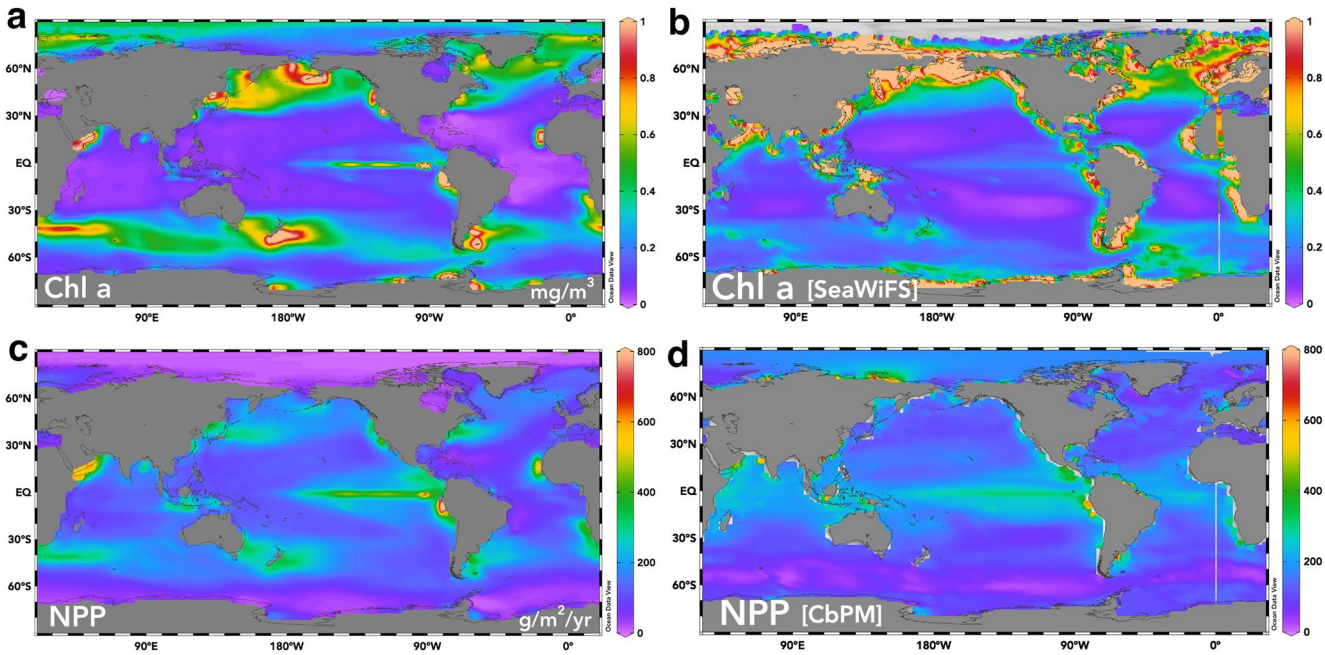

Figure 1. PICO simulated and remotely sensed chlorophyll *a* and net primary productivity (NPP). (a) 20-year averaged sea surface chlorophyll *a* [mg m^{-3}] from PICO, (b) climatological average sea surface chlorophyll *a* from the SeaWiFS satellite during 1997–2010, (c) PICO simulated 20-year averaged NPP [g C m^{-2} yr^{-1}], and (d) from the CbPM model using SeaWiFS satellite data from the same era (Westberry et al., 2008).

Simulated pico-phytoplankton biomass are validated against the data assimilative niche modeling of Flombaum et al. (2013, 2020) that predicts field observed *Prochlorococcus*, *Synechococcus* from inputs of temperature and irradiance (Flombaum et al., 2013) and pico-eukaryote biomass from inputs of temperature, irradiance, and dissolved nitrate (Flombaum et al., 2020). Pico-phytoplankton biomass and C:P stoichiometry are compared against field observations of flow-sorted populations from the North Atlantic, eastern Pacific, and eastern Indian Oceans of *Prochlorococcus*, *Synechococcus*, and pico-eukaryotes measured for C and P content (Baer et al., 2017; Lomas et al., 2021). Simulated total phytoplankton biomass C:P stoichiometry is compared with a global compilation of bulk particulate organic matter C, N, and P content (Martiny et al., 2014). Total simulated pico-phytoplankton (pro + syn + peuk + diaz), nano-phytoplankton, and micro-phytoplankton (diat) from PICO are compared with a remote sensing (SeaWiFS) climatology of combined pico-, nano-, and micro-sized phytoplankton biomass (Brewin, 2012).

3. Results

3.1. Chlorophyll *a* and NPP

Sea surface chlorophyll *a* (chl *a*) concentrations [mg m^{-3}] from the PICO simulation and the SeaWiFS satellite climatology are shown in Figures 1a and 1b. BEC simulated chl *a* captures the overall pattern of lowest concentrations within the subtropical ocean gyres, highest concentrations within coastal and subpolar zones, and intermediate concentrations in upwelling regions and subtropical to mid-latitude transition zones (Figure 1). The PICO simulation exhibits an overall global negative mean bias (defined as the average difference between model predicted and observed quantities, expressed as a percentage) in chl *a* (−6%; Table 2) relative to the SeaWiFS climatology, reducing by a factor of ∼3 compared with the 3 PFT variable C:P stoichiometry BEC model (VAR-3) and an earlier version containing 3 PFTs and Redfield stoichiometry (RED-3) (Table 2).

Vertically integrated annual NPP [g C m^{-2} yr^{-1}] from the PICO simulation is provided along with the Carbon-based Productivity Model estimate of NPP from the SeaWiFS climatology (Westberry et al., 2008) (Figures 1c and 1d). The globally integrated annual NPP from PICO is 51.4 ± 0.75 Pg C yr^{-1}, within the range of satellite-based estimates—60–67 Pg C yr^{-1} (Behrenfeld et al., 2005), 52 Pg C yr^{-1} (Silsbe et al., 2016; Westberry et al., 2008), 58 ± 7 Pg C yr^{-1} (Buitenhuis et al., 2013). The highest rates of annual NPP are simulated in the equatorial Pacific,

Table 2
Comparison Metrics for PICO, VAR-3, and RED-3 Simulated Chlorophyll a and Net Primary Productivity Versus Satellite (SeaWiFS) Climatology Estimates Using the CbPM Model

	PICO		VAR-3		RED-3	
	r-correlation	Mean bias	*r*-correlation	Mean bias	*r*-correlation	Mean bias
Chl a	0.087	−6%	0.218	−19%	0.167	−17%
CbPM NPP	0.241	+3%	0.108	+0.5%	0.153	−3.0%
$[NO_3^-]$	0.938	0.01 μM	0.940	0.01 μM	0.920	0.01 μM
$[PO_4^{3-}]$	0.940	0.02 μM	0.932	−0.01 μM	0.944	0.03 μM
$[SiO_4^{4-}]$	0.935	0.01 μM	0.936	1.14 μM	0.932	−0.01 μM
[dFe]	0.398	0.18 nM	0.332	−0.14 nM	0.374	0.04 nM

Note. Metrics for dissolved nutrients from the same three simulations are compared versus the World Ocean Atlas 2013 (NO_3^-, PO_4^{3-}, SiO_4^{4-}) and Tagliabue et al. (2012) Fe data compilation.

Arabian Sea, and the South Pacific and North Atlantic eastern boundary upwelling zones, reaching rates of ∼400–600 g C m^{-2} yr^{-1} in the PICO simulation, which is approximately 25%–75% greater than those estimated by the CbPM. The lowest rates of NPP simulated by PICO are found within the Arctic Ocean, which are approximately one-quarter of those estimated by CbPM. The PICO simulation also simulates higher rates of NPP as compared to CbPM within the mid-latitudes of both hemispheres, especially near the western boundary of each ocean basin. Overall, the PICO simulation exhibits a small positive mean bias of +3% in estimated global annual NPP rates when comparing binned 3° × 3° pixels with the CbPM SeaWiFS climatology (Table 2), albeit with a relatively poor correlation coefficient, not uncommon for comparing ESM output against remote sensing-based products of NPP and chl *a* (Bopp et al., 2013; Kwiatkowski et al., 2020).

3.2. PFT Contributions to Spatial NPP Patterns

The fractional contribution of each of the six PFTs to simulated NPP rates within the PICO simulation is shown in Figure 2. The majority of NPP within the five subtropical gyre regions is contributed by *Prochlorococcus* (fraction of NPP ∼0.50–0.90), with a general western intensification (Figure 2a). *Synechococcus* NPP is similarly elevated within the subtropics, albeit at lower fractional contributions in the range ∼0.06–0.12 (Figure 2b). *Prochlorococcus* and *Synechococcus* are mostly absent from the polar oceans due to their imposed temperature threshold of 13 and 4°C for positive growth rates (Flombaum et al., 2013; Table 1). Pico-eukaryotes dominate NPP (fraction of NPP > 0.80) in many of the eastern boundary and mid-latitude regions of the world ocean in PICO (Figure 2c). Elsewhere, pico-eukaryote contribution to simulated NPP is much reduced, in the range

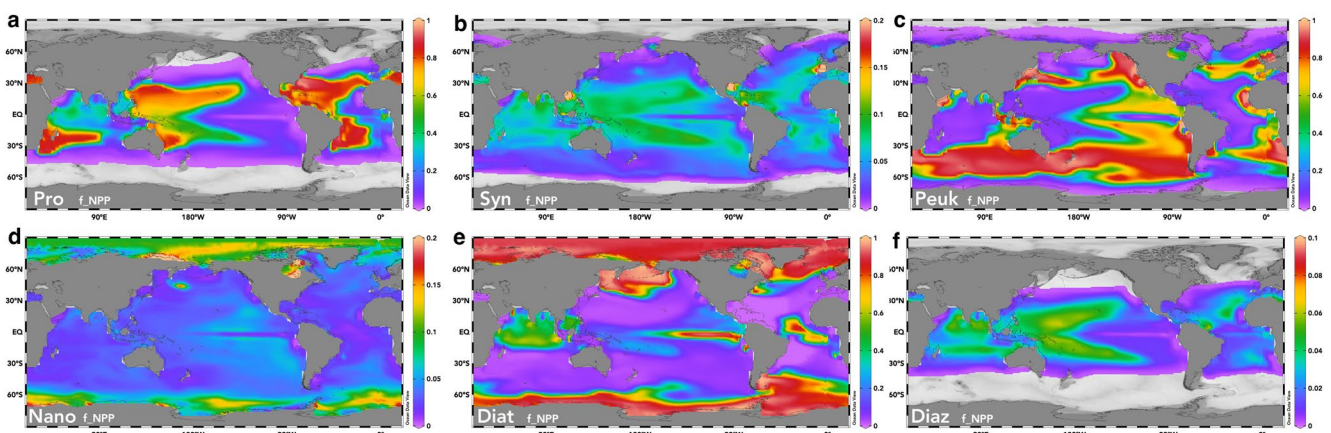

Figure 2. Fraction of vertically integrated, annual marine net primary productivity attributable to each phytoplankton functional type from the PICO simulation. (a) *Prochlorococcus*, (b) *Synechococcus*, (c) pico-eukaryotes, (d) nano-phytoplankton, (e) diatoms, (f) diazotrophs. Note the change in range in panels a, c, e from panels b, d, and panel (f).

Table 3
Comparison Metrics for PICO Simulated Pico-Phytoplankton Biomass Versus the Data Assimilative Niche Models of Flombaum et al. (2013, 2020) (Pro C Niche, Syn C Niche, Peuk C Niche); Versus Pico-Phytoplankton Biomass C:P Stoichiometry (Baer et al., 2017; Lomas et al., 2021) (Pro C:P, Syn C:P, Peuk C:P) and Biomass C (Pro C, Syn C, Peuk C); Versus Bulk Particulate Organic Matter C:P Stoichiometry (Martiny et al., 2014) (POC:POP), and Versus a Remote Sensing Estimate of Combined Pico-, Nano-, and Micro-Sized Phytoplankton Biomass (Pico C, Nano C, Micro C; Brewin, 2012)

	r-correlation	Mean bias	*n*
Pro C niche	0.637	−56%	24,447
Syn C niche	0.459	−85%	33,101
Peuk C niche	0.485	−76%	39,244
Pro C:P	0.120	−5.6%	55
Syn C:P	0.229	−17.1%	44
Peuk C:P	0.021	+11.1%	50
POC:POP	0.245	+20%	4,651
Pro C	0.199	+76%	2,188
Syn C	0.245	−72%	4,120
Peuk C	0.142	−72%	4,158
Pico C	0.476	+2.8%	7,490
Nano C	0.096	−31%	7,755
Micro C	0.399	+24%	7,413

~0.02–0.10. Nano-phytoplankton contribute variably to NPP rates within a range of 0.02–0.20 throughout the world ocean in PICO (Figure 2d). The lowest simulated contributions are found in the eastern and equatorial upwelling regions; the highest contributions are located in the polar oceans. Diatoms dominate simulated NPP rates (fraction > 0.80) within the subpolar and polar oceans as well as the equatorial Pacific (Figure 2e), with the lowest fractional contributions to NPP (~0.01–0.05) located within the subtropical gyres. Diazotrophs contribute <0.07 to simulated NPP rates and are absent from the subpolar and polar oceans due to the imposed minimum temperature of 18°C for positive growth rates (Table 1). The highest diazotroph contributions to NPP rates are found within the western tropical to subtropical North and South Pacific Oceans (~0.04–0.07) (Figure 2f), similar to other OBGC model simulations that incorporate variable nutrient stoichiometry (e.g., Wang et al., 2019).

3.3. Nutrients

Upper ocean (0–500 m) simulated dissolved nutrient concentrations from PICO have been compared with the WOA 2013 climatology (H. E. Garcia et al., 2013) for nitrate (NO_3^-), phosphate (PO_4^{3-}), and silicate (SiO_4^{4-}) and a global compilation of dissolved Fe (dFe) measurements (Tagliabue et al., 2012). Table 2 provides the *r*-correlation parameter and mean bias (μM) from a regression of log-transformed model-observation pairs. Dissolved NO_3^-, PO_4^{3-}, and SiO_4^{4-} are equally well correlated with WOA nutrients, exhibiting *r*-correlation coefficients of ~0.94 and mean biases of +0.01 μM NO_3^-, +0.02 μM PO_4^{3-}, and +0.01 μM SiO_4^{4-}. PICO-simulated dFe is the most weakly correlated nutrient with observational data, $r = 0.40$, with a mean bias of +0.18 nM. The PICO upper ocean dissolved nutrient mean biases are similar to those of the other variable C:P stoichiometry simulation, VAR-3, and the Redfield simulation, RED-3, with a notable improvement to the mean bias of SiO_4^{4-} from VAR-3 (Table 2).

3.4. Biomass

PICO simulated biomass (μmol C L^{-1}) is compared with the data assimilative niche model output for *Prochlorococcus* and *Synechococcus* (Flombaum et al., 2013) and pico-eukaryotes (Flombaum et al., 2020) binned by 3° × 3° pixels. Simulated pico-phytoplankton biomass correlation coefficients with the niche model output range from 0.485 (pico-eukaryotes) to 0.637 (*Prochlorococcus*) (Table 3). However, significant negative biases are present within PICO simulated *Prochlorococcus* biomass (−56%), *Synechococcus* biomass (−85%), and pico-eukaryotes biomass (−76%) (Table 3). PICO pico-phytoplankton biomass has also been compared with a globally compiled field-based data set of flow-sorted populations (Baer et al., 2017; Lomas et al., 2021), yielding metrics of *Prochlorococcus* biomass (+76%, $r = 0.199$), *Synechococcus* biomass (−72%, $r = 0.245$), and pico-eukaryotes biomass (−72%, $r = 0.142$) (Table 3). The regions with the most significant *Prochlorococcus* overestimates in PICO include the central Indian Ocean and the northern half of the subtropical North Atlantic gyre (Figure 3a). Significant *Synechococcus* and pico-eukaryotes underestimates in PICO are found in the central Indian Ocean, the Peruvian upwelling, the subarctic North Atlantic, and the Chukchi Sea (Figures 3b and 3c).

3.5. Phytoplankton Stoichiometry

Euphotic zone-averaged PFT C:P stoichiometry from the PICO simulation is shown in Figure 4. *Prochlorococcus* (Figure 4a) and diazotrophs (Figure 4f) exhibit the greatest range in cellular C:P stoichiometry, with the minimum stoichiometry found within the eastern equatorial Pacific Ocean, C:P = ~90 for pro and C:P = ~150 for diaz, increasing to maximum cellular C:P = ~250–300 within the North and South Atlantic subtropical gyres. Elevated C:P stoichiometry for *Prochlorococcus* and diazotrophs is also found within the other three subtropical gyre regions, with typical values in the range ~180–300. *Synechococcus* (Figure 4b), pico-eukaryotes (Figure 4c),

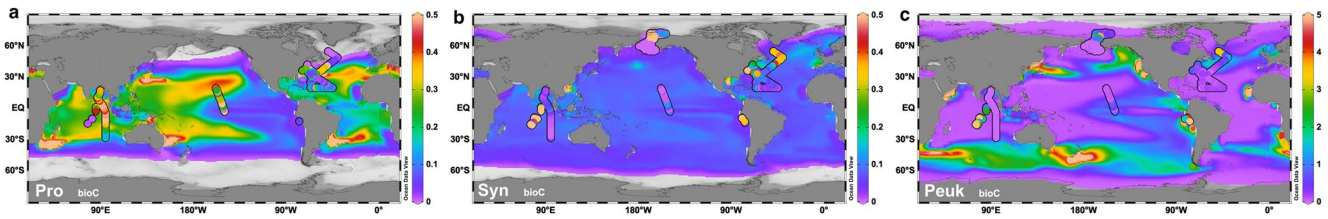

Figure 3. Euphotic zone averaged biomass (μM C) for pico-phytoplankton from the PICO simulation (color mapping) compared to field observations from Baer et al. (2017) and Lomas et al. (2021) (colored dots). (a) *Prochlorococcus*, (b) *Synechococcus*, (c) pico-eukaryotes.

nano-phytoplankton (Figure 4d), and diatoms (Figure 4e) all exhibit similar geographical variability in cellular C:P stoichiometry to *Prochlorococcus* and diazotrophs, with elevated values typical of the five subtropical ocean gyre regions, syn C:P = ~150–210; peuk + nano + diat C:P = ~110–125. Phytoplankton C:P stoichiometry is ~25%–80% more elevated within the western half of each subtropical gyre relative to the eastern half.

PICO simulated *Prochlorococcus*, *Synechococcus*, and pico-eukaryotes cellular C:P stoichiometry has been compared with a subset of the cell-sorted population data set for which biomass P was measured (Baer et al., 2017; Lomas et al., 2021). PICO simulated *Prochlorococcus* C:P exhibits the smallest mean bias of −6% below the average field-based estimate of C:P = 221 (Table 3). PICO simulated *Synechococcus* C:P has a negative mean bias of −17% below the field estimate of 187. PICO simulated pico-eukaryotes exhibited a positive mean bias compared to field estimates at +11% above the field estimate of 103. PICO simulated total autotrophic biomass C:P stoichiometry is compared with a global compilation of surface ocean suspended organic matter C:P stoichiometry (Martiny et al., 2014), exhibiting a positive mean bias of +20% above the field-based estimate of POC:POP = 171:1 (Table 3).

3.6. Sinking Carbon Export

The sinking particulate organic carbon flux through the 100 m depth horizon ($POC_{exp,100m}$) from the PICO simulation is plotted in Figure 5a. $POC_{exp,100m}$ exhibits a similar geographical distribution as simulated NPP (Figure 1c), with maximum rates of ~90–120 g C m^{-2} yr^{-1} found within the eastern equatorial Pacific, Peruvian, and Arabian Sea upwelling regions as well as the SW Atlantic Ocean and minimum rates, <20 g C m^{-2} yr^{-1}, within the five subtropical ocean gyres and their bordering tropical regions, the Southern Ocean, and the Arctic Ocean. Other regions exhibiting elevated $POC_{exp,100m}$ include the eastern boundary upwelling zones and the subtropical to mid-latitude transition zones with rates in the range ~40–70 g C m^{-2} yr^{-1}. The pico-phytoplankton contribution to $POC_{exp,100m}$ is greatest across the tropics, subtropics, and mid-latitudes (Figure 5b), with a fractional contribution in the range ~0.50–0.70. In both hemispheres, pico-phytoplankton make their largest contribution to sinking POC export in the mid-latitudes (~40–50°N and °S), approaching 65%–70% of $POC_{exp,100m}$, with minima (~0.10–0.30) estimated for the subpolar, polar, and equatorial Pacific Oceans. The globally integrated

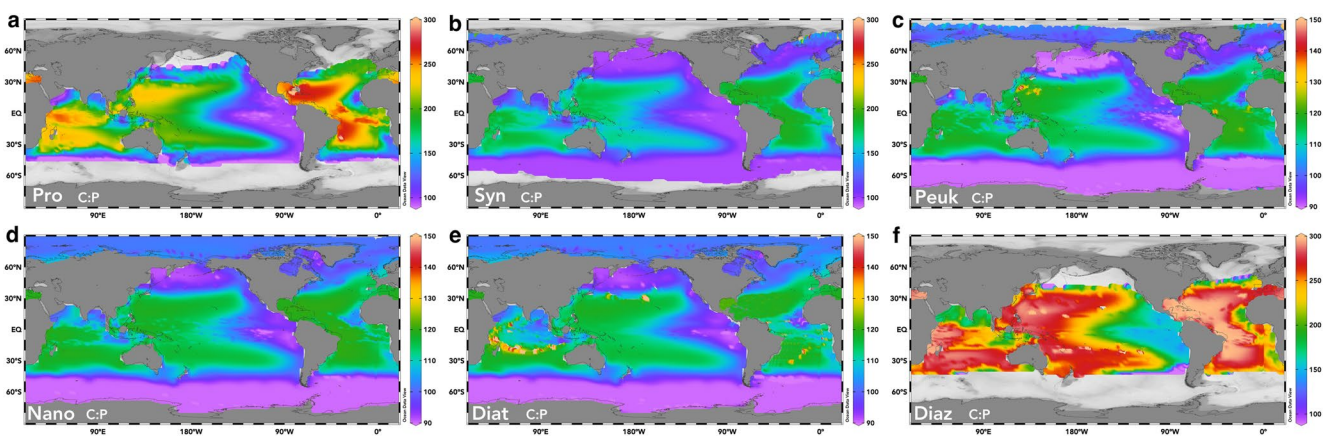

Figure 4. Euphotic zone averaged cellular C:P stoichiometry for each phytoplankton functional type from the PICO simulation. (a) *Prochlorococcus*, (b) *Synechococcus*, (c) pico-eukaryotes, (d) nano-phytoplankton, (e) diatoms, (f) diazotrophs.

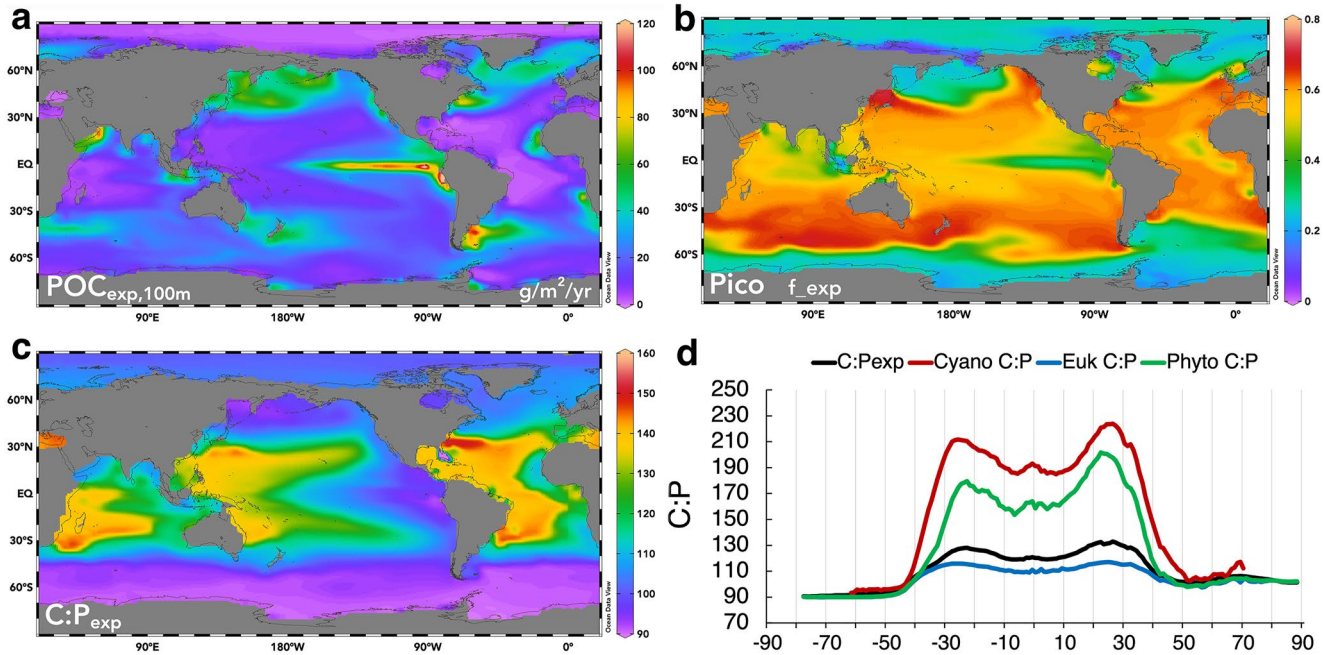

Figure 5. PICO simulated carbon export and its stoichiometry. (a) 20-year averaged sinking particulate organic carbon export below 100 m $POC_{exp,100m}$ [g C m^{-2} yr^{-1}], (b) the fraction of total $POC_{exp,100m}$ attributable to pico-phytoplankton (pro + syn + peuk), (c) the C:P stoichiometry of sinking organic particles $C:P_{exp}$ at 100 m, and (d) the zonal mean $C:P_{exp}$ at 100 m (black line), C:P of cyanobacteria (pro + syn + diaz; red line), C:P of eukaryotic phytoplankton biomass (peuk + nano + diat; blue line), and C:P of total phytoplankton (green line) within the upper 100 m.

$POC_{exp,100m}$ flux below 100 m from PICO is 7.0 ± 0.1 Pg C yr^{-1}; within the range of observational-, satellite-, and model-based estimates of global marine export production, for example, 4–14 Pg C yr^{-1} (summarized in Emerson (2014), Britten and Primeau (2016), Siegel et al. (2014), and Henson et al. (2011)). It should be noted that when comparing the PICO carbon export flux to other estimates from the literature that dissolved organic carbon export below 100 m contributes an additional ∼2.1 Pg C yr^{-1} of carbon export production in the BEC model (Letscher & Moore, 2015; Letscher et al., 2015) bringing estimated total organic carbon export below 100 m to ∼9.1 Pg C yr^{-1}.

The C:P stoichiometry of the sinking organic particulate flux at 100 m ($C:P_{exp}$) from the PICO simulation is shown in Figure 5c. Carbon rich/P-poor stoichiometry for $C:P_{exp}$ is found in the ocean tropics and subtropics, being a function of both the large contribution of pico-phytoplankton productivity (Figure 2) in these regions as well as the elevated C:P stoichiometry of the cyanobacteria (pro + syn + diaz) PFTs inhabiting these regions (Figure 5d). Sinking particulate export C:P stoichiometry exhibits global maxima within the western subtropical gyres of each basin, reaching values of ∼140–150 (Figure 5c). C:P export stoichiometry is elevated elsewhere within the subtropics, ∼120–140, near Redfieldian in the mid-latitudes and the Arctic Ocean, and depressed within the eastern equatorial Pacific, subpolar North Pacific, and the Southern Ocean, exhibiting values in the range ∼90–105. The zonal mean $C:P_{exp}$ is near the minimum imposed value of 90 for eukaryotic phytoplankton groups south of 50°S and near ∼100 north of 50°N where the phytoplankton community is dominated by diatoms and other eukaryote groups (Figure 2). Maximal zonal mean $C:P_{exp}$ is found at subtropical latitudes exhibiting values of ∼128 at 23°S and a slightly higher value of ∼133 at 26°N in the northern hemisphere (Figure 5d). Cyanobacteria phytoplankton (pro + syn + diaz), eukaryotic phytoplankton (peuk + nano + diat), and the total phytoplankton community C:P stoichiometry all exhibit similar latitudinal patterns with high latitude minima and subtropical maxima (Figure 5d). Cyanobacteria phytoplankton C:P varies between ∼96–223, and eukaryotic phytoplankton C:P varies between ∼90–117, with total phytoplankton C:P varying between ∼90–202.

4. Discussion

Simulated pico-phytoplankton were found to make their largest contribution to marine NPP within the tropical and subtropical oceans, reaching contributions of ∼50%–90% within the latitudinal range 45°N–45°S (Figure 2).

Table 4
Percentages of Globally Integrated Marine NPP, $POC_{exp,100m}$, and pge-ratio (% of Cexp/% of NPP = Phytoplankton Group Export Ratio) Attributable to Each Phytoplankton Functional Type for the PICO, VAR-3, and RED-3 Simulations

	PICO			VAR-3			RED-3			Literature
PFT	% of NPP	% of POCexp	pge-ratio	% of NPP	% of POCexp	pge-ratio	% of NPP	% of POCexp	pge-ratio	pge-ratio
Prochlorococcus	16.6	14.9	0.90	–	–	–	–	–	–	0.17 ± 0.14[a]
Synechococcus	3.9	12.6	3.2	–	–	–	–	–	–	0.30 ± 0.17[a,b,c]
Pico-eukaryotes	37.1	18.1	0.49	–	–	–	–	–	–	1.8 ± 1.3[a,c,d]
Nano-phytoplankton	3.6	9.9	2.8	–	–	–	–	–	–	1.3 ± 0.5[e,f]
Diatoms	37.5	31.2	0.83	50.2	68.0	1.35	29.7	63.3	2.1	1.7 ± 0.6[e,f]
Diazotrophs	1.2	13.4	11.2	2.3	14.4	6.26	1.2	15.0	12.5	–
Σ Pico-phytoplankton	57.6	45.6	0.79	–	–	–	–	–	–	0.91 ± 0.21[e,f]
Σ Small phytoplankton	61.2	55.5	0.91	47.5	17.5	0.37	69.1	21.7	0.31	–

Note. Literature estimates of the pge-ratio are provided, ± is 1 S.D. of the mean of multiple field-based estimates.
[a]Lomas and Moran (2011). [b]Stukel et al. (2013). [c]Fawcett et al. (2011). [d]Stukel and Landry (2010). [e]Richardson and Jackson (2007). [f]Richardson (2019).

In general, *Prochlorococcus* dominates NPP within the subtropical gyre regions, particularly the western halves, transitioning to dominance by pico-eukaryotes equatorward, eastward, and poleward of ∼30° latitude to ∼45°. *Synechococcus* follows a similar spatial pattern as *Prochlorococcus* but never dominates the phytoplankton community, with fractional contributions peaking at ∼10%–12% in the subtropical gyres. The spatial pattern obtained for pico-phytoplankton and diatom contributions to marine NPP is in general agreement with a remote sensing-based estimate by Uitz et al. (2010) with some overestimates in the regions of highest relative inputs by pico-phytoplankton and diatoms in PICO. Diazotrophs, which are parameterized to represent the cyanobacteria lineages of *Trichodesmium* and *Crocosphaera* in the BEC model, make a smaller yet important additional contribution in these same low-latitude regions. The pico-phytoplankton and diazotroph groups within the PICO simulation were assigned the largest cellular C:P plasticity and higher minimum temperature thresholds for growth (Table 1) than the larger nano-phytoplankton and diatoms, with the pico-phytoplankton niche being realized within the nutrient-poor high temperature waters of the low latitudes. The three pico-phytoplankton PFTs in PICO contributed to globally integrated NPP at a percentage of 16.6% ± 0.4% for *Prochlorococcus*, 3.9% ± 0.5% for *Synechococcus*, and 37.1% ± 0.6% for pico-eukaryotes, for a total pico-phytoplankton contribution of 57.6% ± 0.8% to marine NPP (Table 4). These estimates for global NPP attributable to *Prochlorococcus* and *Synechococcus* within PICO are approximately double and one-quarter, respectively, compared to an independent estimate based on data assimilative modeling of niche partitioning (pro = 8.5%, syn = 16.7%, Flombaum et al., 2013); however, both model estimates converge on a combined pro + syn contribution to marine NPP of ∼20%–25%. The PICO simulated pico-phytoplankton biomass distributions (Figure 3) generally match the niche separation predicted by Flombaum et al. (2013, 2020) with *Prochlorococcus* dominating in the western subtropical gyre regions, possibly due to their diagnosed affinity for the warmest temperatures (Flombaum et al., 2013), *Synechococcus* occupying a more spatially broad distribution across the subtropical and mid-latitudes, and pico-eukaryote abundance peaking in the eastern subtropics, gyre margins, and mid-latitudes, possible owing to their diagnosed higher affinity for environments with measurable nitrate (Flombaum et al., 2020). Nano-phytoplankton contribute 3.6% ± 0.7% of global NPP in PICO, an underestimate, for example, Brewin et al., 2010; Uitz et al., 2010; Juranek et al., 2020, concentrated in the Southern Ocean, the subpolar and Arctic Ocean, as well as the eastern tropical Pacific Ocean (Figure 2d). Diatoms are the largest contributor to global marine NPP in PICO, contributing 37.5% ± 0.5%, concentrated in the subpolar and polar oceans as well as the equatorial Pacific upwelling (Table 4; Figure 2d). This rate of diatom contribution to global NPP is consistent with the ∼38%–43% contribution estimated from marine biogenic silica budgets (Nelson et al., 1995). Diazotrophs contribute 1.2% ± 0.04% to marine NPP in PICO (Table 4), concentrated in the same tropical and subtropical regions as pico-phytoplankton, especially the western tropical and subtropical Pacific Ocean (Figure 2e).

Ecosystem processing of the newly fixed organic matter by each phytoplankton PFT contributes to the detrital particulate organic matter pools, which constitute the source terms to the sinking export fluxes of POC_{exp} and particulate organic phosphorus (POP_{exp}) in the BEC model. These processes include losses to the detrital pool upon grazing by zooplankton, zooplankton contributions to the detrital pool as a result of grazing (e.g., fecal pellet production), and aggregation and sinking of phytoplankton biomass upon cell mortality within the BEC model (Moore et al., 2004). The parameter values governing these processes were prescribed in a size-scaling manner across the six PFTs in PICO (Table 1), with the pico-phytoplankton contributing the smallest to the particulate sinking fluxes, increasing with diazotrophs and nano-plankton to the largest contribution from diatoms. The fractions of pico-phytoplankton grazing and zooplankton losses that accumulate within the particulate fluxes were prescribed in the range 0.07–0.33 (Table 1), at the upper end of estimates based on pigment biomarker analyses of the sediment trap

flux collected from the Sargasso Sea (Lomas & Moran, 2011). Higher estimates for pico-phytoplankton detrital contributions were needed to export enough N and P below the euphotic zone to prevent spurious accumulation of NO_3^- and PO_4^{3-} concentrations in the upper layers of the subtropics. The nano-phytoplankton and diatom contributions to NPP are <5% each over much of the subtropical regions in PICO (Figure 2), which are biased low compared to field observations (e.g., Brzezinski et al., 2011; Juranek et al., 2020; Nelson & Brzezinski, 1997) and may potentially explain the low N and P export efficiency, partially satisfied by prescribed elevated pico-phytoplankton detrital contributions in PICO. PFT-specific parameters linked to the detrital contributions are held constant in PICO, however future formulations of the BEC model (now called the Marine Biogeochemistry Library, MARBL) could include parameterizations that are dependent on in situ temperature, PFT growth rate, grazing rate, or nutrient limitation status among others.

Within PICO, pico-phytoplankton contribute nearly half (45.6% ± 0.3%) of the globally integrated $POC_{exp,100m}$ flux through 100 m when accounting for both direct (e.g., aggregation) and indirect (e.g., zooplankton processing of pico-produced organic matter) contributions. Approximately 40% of the pico-phytoplankton total is contributed by pico-eukaryotes (18.1% ± 0.2%), an additional third contributed by *Prochlorococcus* (14.9% ± 0.1%), and a quarter contributed by *Synechococcus* (12.6% ± 0.1%) (Table 4). Pico-phytoplankton dominate the phytoplankton contribution to carbon export across large areas of the tropics, subtropics, and mid-latitudes (Figure 5b), which is an emergent result from the added phytoplankton biodiversity, their competition for limiting nutrients, the represented cellular stoichiometric diversity, and ecosystem processing of the detrital pool mediated by zooplankton grazing. Perhaps counterintuitively, pico-phytoplankton contribution to carbon export peaks in importance (~0.65–0.7), not where their greatest environmental niche is realized, that is, the high light and low nutrient waters of the oligotrophic subtropical gyres, but at mid-latitudes, ~35–45°, driven largely by regional maxima in C:P stoichiometry (Figure 5c). Thus, pico-phytoplankton biodiversity and stoichiometric diversity combined are important controls on marine carbon export patterns, expanding the oceanic provinces exhibiting significant export (Figure 5) and diminishing the strong latitudinal gradients in the strength of the biological carbon pump predicted by previous models that represent less phytoplankton biodiversity with Redfield stoichiometry (e.g., Emerson, 2014 and references therein).

The estimate of pico-phytoplankton contribution to sinking carbon export in PICO (~46%) is approximately 80% their combined contributions to global NPP (~58%), in agreement with inversions of PFT-specific observational data from the equatorial Pacific and Arabian Sea suggesting that pico-phytoplankton contribute to carbon export at rates comparable to their contribution to NPP (Richardson, 2019; Richardson & Jackson, 2007). Phytoplankton group specific C export fraction to NPP fraction ratios (which we define the phytoplankton group export ratio, pge-ratio), presented in Table 4, range from a minimum of ~0.5 to ~3.2, within the range of the available group-specific estimates diagnosed from a range of field data, ~0.1 to ~3.1 (Fawcett et al., 2011; Lomas & Moran, 2011; Richardson, 2019; Richardson & Jackson, 2007; Stukel et al., 2013; Stukel & Landry, 2010), albeit at the higher end especially for Pro and Syn which are 0.9 and 3.2 in PICO and 0.17 ± 0.14 and 0.30 ± 0.17 from the literature (Fawcett et al., 2011; Lomas & Moran, 2011; Stukel et al., 2013), respectively. A notable outlier is the pge-ratio for diazotrophs which is ~11 in PICO but lacks a literature estimate to help constrain. Dissolved organic matter (DOM) contributes ~20%–25% of total organic carbon export production in the CESM (Letscher et al., 2015). We are unable to provide an estimate of each PFT contribution to the DOM export flux as DOM export is spatially and temporally offset from its region of production, and the model does not track DOM sourced from individual PFTs. Each PFT contributes a constant fraction of its newly produced organic matter to the DOM pool; therefore, PFT contributions to DOM export should generally track the proportions of PFT contributions to NPP (e.g., Table 4).

The pge-ratio for diatoms is 0.83 and 0.91 for the sum of the small phytoplankton (e.g., pro + syn + peuk + nano) in PICO (Table 4). The group-specific pge-ratio in the RED-3 version of the BEC, which represents 3 PFTs with Redfield stoichiometry, exhibits quite different group-specific pge-ratios, with carbon export dominated by the diatoms (pge-ratio = 2.1) and a much-reduced contribution from small phytoplankton (pge-ratio = 0.3; Table 4). Adding a representation of phytoplankton stoichiometric diversity in VAR-3 alters these group-specific pge-ratios toward a slightly higher contribution from small phytoplankton (e.g., 0.37 vs. 0.31) and lower contribution from diatoms (e.g., 1.4 vs. 2.1). Small versus large phytoplankton pge-ratios are significantly altered by the additional representation of pico-phytoplankton biodiversity in PICO with pico-sized, "small"-sized, and diatom e-ratios approaching unity. This result, that the group-specific pge-ratio approaches unity in PICO indicates that enhanced representation of the biodiversity and stoichiometric diversity of marine phytoplankton significantly alters the

sensitivity of the biological carbon pump to changes in phytoplankton community composition and nutrient supply in this model. These combined effects could mute the predicted decline in 21st century marine NPP and carbon export fluxes (Bopp et al., 2013; Kwiatkowski et al., 2020) as shifts to smaller sized phytoplankton with higher plasticity in cellular nutrient to carbon stoichiometry may occur. These predictions await the future evolution of the marine ecosystem and targeted field sampling campaigns to confirm.

The regions located immediately along the poleward and western edges of the surface western boundary currents of the subtropical gyre regions of each ocean basin exhibit elevated $POC_{exp,100m}$ fluxes on the order of ∼50–90 g C m^{-2} yr^{-1} (Figure 5a), approximately ∼2–3 fold higher as compared to the adjacent regions. These so-called "gyre recirculation regions" of the surface western boundary currents are characterized by strong eddying flow and enhanced lateral nutrient concentration gradients that stand out as important regions for the delivery of a lateral nutrient flux that dominates nutrient resupply to the subtropical gyres (Jenkins & Doney, 2003; Letscher et al., 2016; Oschlies, 2002; Palter et al., 2013; Torres-Valdés et al., 2009; Williams & Follows, 1998; Yamamoto et al., 2018). The resolution of the BEC model employed in PICO is non-eddy resolving; however, it is able to simulate somewhat elevated rates of NPP (Figure 1a) and associated $POC_{exp,100m}$ (Figure 5a) along these subtropical to subpolar gyre flanks at the western side. These gyre recirculation region biogeochemical features are driven by a larger contribution of pico-eukaryotes and diatoms to simulated NPP (Figure 2). These regions are also where PFT cellular C:P stoichiometry transitions from C-rich/P-poor stoichiometry within the subtropical gyres to more Redfield-like C:P stoichiometry poleward (Figures 4, 5c, and 5d). Thus, the magnitude of $POC_{exp,100m}$ within the subtropical gyre recirculation regions identified as "POC_{exp} hotspots" by PICO may be sensitive to small changes to the nutrient flux stoichiometry which drive cellular C:P stoichiometry. Further field-based studies of the in situ phytoplankton community composition and associated biomass C:P stoichiometry within these regions could help confirm their regional "POC_{exp} hotspot" status.

The PICO simulation builds from recent advances in a BEC model formulation that added variable C:P stoichiometry within the three traditionally simulated PFTs (small phytoplankton, diatoms, diazotrophs; Wang et al., 2019) by adding three pico-phytoplankton PFTs with variable C:P stoichiometry. As compared to the variable C:P in the three PFT versions of the BEC model (VAR-3; Wang et al., 2019), the PICO simulation exhibits ∼1% higher globally integrated NPP (51.4 vs. 50.8 Pg C yr^{-1}) and ∼18% lower $POC_{exp,100m}$ (7.0 vs. 8.5 Pg C yr^{-1}). Thus, given that both the three and six PFT, variable C:P formulations of the BEC model reproduce similarly well, the surface to deep ocean spatial gradients in dissolved nutrient concentrations (Table 2), the pico-phytoplankton enabled (6p1z) BEC model predicts similar rates of NPP, with lower rates of $POC_{exp,100m}$, and lower $C:P_{exp}$ per unit of phosphorus utilized within the euphotic zone as compared with the three PFT BEC model versions (VAR-3; Wang et al., 2019). The geographical distribution of $POC_{exp,100m}$ is similar between the PICO and VAR-3 simulations; however, VAR-3 simulated $POC_{exp,100m}$ is approximately double to triple that estimated by PICO within the subtropics to mid-latitudes (not shown), contributing to its overall ∼18% higher estimate of global $POC_{exp,100m}$. The lower $POC_{exp,100m}$ estimate using the PICO model is likely attributable to the lower prescribed values of zooplankton grazing routed to the particulate organic pool, "graze_poc" parameter, for the pico PFTs (graze_poc = 0.07–0.13; Table 1) versus the small phytoplankton PFT in Wang et al. (2019) (graze_poc = 0.3). Maximum $C:P_{exp}$ is estimated within the ocean's subtropical gyres (Figure 5c) in both simulations, with PICO predicting slightly lower maximum $C:P_{exp}$ within the Indo-Pacific subtropics, ∼140–145 versus ∼180 in VAR-3 (not shown). PICO-simulated $C:P_{exp}$ generally agrees with the spatial pattern estimated from an inversion of dissolved inorganic carbon and phosphate data (Teng et al., 2014), with notable differences in $C:P_{exp}$ magnitude. PICO minimum PFT C:P is set at 90 while the Teng et al. (2014) inversion estimates minimum $C:P_{exp}$ of ∼60–100 for the equatorial and subpolar regions. Maximal $C:P_{exp}$ in the subtropical North Atlantic is ∼155 in PICO compared to ∼355 by Teng et al. (2014). These comparisons demonstrate that estimates of the globally important fluxes of marine NPP and carbon export, including its C:P stoichiometry, vary on the order of ∼10%–50% between OBGC model formulations, highlighting the continued need for observational data sets to further constrain and validate model simulations of ocean biogeochemistry.

We are aware of two other ESMs to which the addition of variable phosphorus to carbon ratios within the OBGC model has been performed as well as an additional global ocean biogeochemistry model. While nearly all ESMs participating in the CMIP5 suite predict declining marine NPP during the 21st century (Bopp et al., 2013), the GFDL-ESM2, which runs the variable C:P enabled TOPAZ2 OBGC model (Dunne, 2013), was the only ESM to predict a resilient rate of marine NPP throughout this century. Presumably the mechanism at play is one in which declining nutrient fluxes to the surface ocean with increasing upper ocean stratification are countered by a switch

in phytoplankton community composition toward smaller, more nutrient plastic types and/or an increase in phytoplankton C:P that allows for the maintenance of carbon-based NPP rates at depressed phosphorus supply fluxes. The PICO simulation presented here supports this interpretation, exhibiting a marginally ∼1% higher overall rate of marine NPP than its analogous three PFT, Redfield C:P sister simulation (RED-3; Letscher & Moore, 2015). Results from a variable C:P OBGC model that added representation of pico-phytoplankton have been published (the PISCES-QUOTA model; Kwiatkowski et al., 2018). The model predicts similar 21st century declines in marine NPP (−8%) and POC_{exp} (−14%) as the fixed (Redfield) stoichiometry ESMs that participated in CMIP5 (Bopp et al., 2013), while noting an increase in carbon export efficiency per unit phosphorus, which increases by 4.5%. The global ocean biogeochemistry modeling study of Tanioka and Matsumoto (2017), in which variable C:P stoichiometry was represented in a two phytoplankton marine ecosystem model, found that predicted declines in global export production could be mitigated by ∼3% relative to a Redfield stoichiometry model over the 21st century that the authors attributed to combined mechanisms of flexible cellular nutrient to carbon ratios and regional shifts in phytoplankton community composition.

5. Future Directions

The PICO simulation provides estimates of the *Prochlorococcus*, *Synechococcus*, and pico-eukaryote biomass and contributions to marine NPP and carbon export at the global scale which should motivate future field sampling efforts to validate or update our understanding of the spatiotemporal patterns of pico-phytoplankton contributions to marine biogeochemistry. Direct field observations of phytoplankton biomass at the population level are still sparse (Figure 3) and there is likely a wealth of information to be learned by continued sampling efforts and population mapping. A next step with the CESM model is to perform a future climate-forced simulation using PICO parameterizations to investigate changes in 21st century marine NPP and carbon export in the context of better represented marine phytoplankton diversity and cellular stoichiometric diversity. We also wish to point out that during the development of the PICO simulation, it was found that the model solution was very sensitive to the choice of the grazing rates for each of the six PFTs by the single zooplankton group. This single zooplankton group formulation was not well suited to act as the top-down control on the growth of six PFTs, with the model exhibiting behavior in which it was difficult to obtain mixed communities of phytoplankton everywhere in the ocean. This was especially true for obtaining a larger contribution for nano-phytoplankton to the mixed phytoplankton community, which is underestimated in PICO. Future improvement of the BEC model, now carried out within the MARBL in CESM v2, should include the addition of explicit nanophytoplankton groups (e.g., coccolithophores) and additional zooplankton groups representing multiple size classes and grazing formulations that will likely result in a more robust simulation of plankton growth, grazing, and export dynamics. Currently, a version with four zooplankton and eight PFTs is in development (8p4z).

Conflict of Interest

The authors declare no conflicts of interest relevant to this study.

Data Availability Statement

The modified BEC model source code used to generate the PICO simulation can be found on Zenodo here: https://zenodo.org/badge/latestdoi/606271192, Letscher. (2023b). The 20-year annually averaged output file for PICO presented in this work is available on Zenodo here: https://zenodo.org/record/8169687, Letscher (2023a).

Acknowledgments
This work was funded by a Grant from the U.S. Dept. of Energy Office of Science #DE-SC0016539 to J.K.M. and R.T.L and OCE-1848576 to A.C.M. R.T.L. also thanks discussions with members of the MARBL development team at NCAR including K. Krumhardt, M. Long, M. Levy, and K. Lindsay as well as M. Maltrud at LANL for advice during the development of the pico-phytoplankton enabled BEC-CESM. P. Flombaum at the University of Buenos Aires is thanked for providing the output of pico-phytoplankton biomass from predictive niche models.

References

Arrigo, K. R., Robinson, D. H., Worthen, D. L., Dunbar, R. B., DiTullio, G. R., VanWoert, M., & Lizotte, M. P. (1999). Phytoplankton community structure and the drawdown of nutrients and CO_2 in the Southern Ocean. *Science*, *283*(5400), 365–367. https://doi.org/10.1126/science.283.5400.365

Aumont, O., Éthé, C., Tagliabue, A., Bopp, L., & Gehlen, M. (2015). PISCES-v2: An ocean biogeochemical model for carbon and ecosystem studies. *Geoscientific Model Development Discussions*, *8*(2), 2465–2513. https://doi.org/10.5194/gmd-8-2465-2015

Baer, S. E., Lomas, M. W., Terpis, K. X., Mouginot, C., & Martiny, A. C. (2017). Stoichiometry of *Prochlorococcus*, *Synechococcus*, and small eukaryotic populations in the western North Atlantic Ocean. *Environmental Microbiology*, *19*(4), 1568–1583. https://doi.org/10.1111/1462-2920.13672

Behrenfeld, M. J., Boss, E., Siegel, D. A., & Shea, D. M. (2005). Carbon-based ocean productivity and phytoplankton physiology from space. *Global Biogeochemical Cycles*, *19*(1). https://doi.org/10.1029/2004gb002299

Berman-Frank, I., Quigg, A., Finkel, Z. V., Irwin, A. J., & Haramaty, L. (2007). Nitrogen-fixation strategies and Fe requirements in cyanobacteria. *Limnology & Oceanography*, *52*(5), 2260–2269. https://doi.org/10.4319/lo.2007.52.5.2260

Bopp, L., Resplandy, L., Orr, J. C., Doney, S. C., Dunne, J. P., Gehlen, M., et al. (2013). Multiple stressors of ocean ecosystems in the 21st century: Projections with CMIP5 models. *Biogeosciences*, *10*, 6225–6245. https://doi.org/10.5194/bg-10-6225-2013

Boyd, P. W., Strzepek, R. F., Ellwood, M. J., Hutchins, D. A., Nodder, S. D., Twining, B. S., & Wilhelm, S. W. (2015). Why are biotic iron pools uniform across high-and low-iron pelagic ecosystems? *Global Biogeochemical Cycles*, *29*(7), 1028–1043. https://doi.org/10.1002/2014gb005014

Brewin, R. J., Lavender, S. J., Hardman-Mountford, N. J., & Hirata, T. (2010). A spectral response approach for detecting dominant phytoplankton size class from satellite remote sensing. *Acta Oceanologica Sinica*, *29*(2), 14–32. https://doi.org/10.1007/s13131-010-0018-y

Brewin, R. J. W. (2012). *Global 10 year monthly climatology and monthly composites of phytoplankton size class from SeaWiFS analyses as part of the national centre for Earth observation (NCEO) theme 2 sub-theme 6*. NERC Earth Observation Data Centre. Retrieved from http://catalogue.ceda.ac.uk/uuid/049ff74d15b0ef759e966b275b8d39bb

Britten, G. L., & Primeau, F. W. (2016). Biome-specific scaling of ocean productivity, temperature, and carbon export efficiency. *Geophysical Research Letters*, *43*(10), 5210–5216. https://doi.org/10.1002/2016gl068778

Brzezinski, M. A., Krause, J. W., Church, M. J., Karl, D. M., Li, B., Jones, J. L., & Updyke, B. (2011). The annual silica cycle of the North Pacific subtropical gyre. *Deep Sea Research Part I: Oceanographic Research Papers*, *58*(10), 988–1001. https://doi.org/10.1016/j.dsr.2011.08.001

Buchanan, P. J., Matear, R. J., Chase, Z., Phipps, S. J., & Bindoff, N. L. (2018). Dynamic biological functioning important for simulating and stabilizing ocean biogeochemistry. *Global Biogeochemical Cycles*, *32*(4), 565–593. https://doi.org/10.1002/2017gb005753

Buitenhuis, E. T., Hashioka, T., & Le Quéré, C. (2013). Combined constraints on global ocean primary production using observations and models. *Global Biogeochemical Cycles*, *27*(3), 847–858. https://doi.org/10.1002/gbc.20074

Buitenhuis, E. T., Li, W. K., Vaulot, D., Lomas, M. W., Landry, M. R., Partensky, F., et al. (2012). Picophytoplankton biomass distribution in the global ocean. *Earth System Science Data*, *4*(1), 37–46. https://doi.org/10.5194/essd-4-37-2012

Cabré, A., Marinov, I., & Leung, S. (2015). Consistent global responses of marine ecosystems to future climate change across the IPCC AR5 earth system models. *Climate Dynamics*, *45*(5–6), 1253–1280. https://doi.org/10.1007/s00382-014-2374-3

Casey, J. R., Lomas, M. W., Michelou, V. K., Dyhrman, S. T., Orchard, E. D., Ammerman, J. W., & Sylvan, J. B. (2009). Phytoplankton taxon-specific orthophosphate (Pi) and ATP utilization in the western subtropical North Atlantic. *Aquatic Microbial Ecology*, *58*(1), 31–44. https://doi.org/10.3354/ame01348

DeVries, T., & Deutsch, C. (2014). Large-scale variations in the stoichiometry of marine organic matter respiration. *Nature Geoscience*, *7*(12), 890–894. https://doi.org/10.1038/ngeo2300

Dunne, J. P. (2013). Technical description of tracers of ocean phytoplankton with allometric zooplankton version 2 (TOPAZ2) used in GFDL's ESM2M and ESM2G submitted as part of the coupled model intercomparison project phase 5. *Journal of Climate*. https://doi.org/10.1175/JCLI-D-12-00150.s1

Dunne, J. P., Gnanadesikan, A., Sarmiento, J. L., Slater, R. D., & Hiscock, M. R. (2010). Technical description of the prototype version (v0) of tracers of phytoplankton with allometric zooplankton (TOPAZ) ocean biogeochemical model as used in the Princeton IFMIP model. *Biogeosciences*, *7*, 3593–3624. https://doi.org/10.5194/bg-7-3593-2010

DuRand, M. D., Olson, R. J., & Chisholm, S. W. (2001). Phytoplankton population dynamics at the Bermuda Atlantic time-series station in the Sargasso Sea. *Deep Sea Research Part II: Topical Studies in Oceanography*, *48*(8–9), 1983–2003. https://doi.org/10.1016/s0967-0645(00)00166-1

Dutkiewicz, S., Cermeno, P., Jahn, O., Follows, M. J., Hickman, A. E., Taniguchi, D. A., & Ward, B. A. (2020). Dimensions of marine phytoplankton diversity. *Biogeosciences*, *17*(3), 609–634. https://doi.org/10.5194/bg-17-609-2020

Dyhrman, S. T., & Ruttenberg, K. C. (2006). Presence and regulation of alkaline phosphatase activity in eukaryotic phytoplankton from the coastal ocean: Implications for dissolved organic phosphorus remineralization. *Limnology & Oceanography*, *51*(3), 1381–1390. https://doi.org/10.4319/lo.2006.51.3.1381

Edwards, K. F., Thomas, M. K., Klausmeier, C. A., & Litchman, E. (2012). Allometric scaling and taxonomic variation in nutrient utilization traits and maximum growth rate of phytoplankton. *Limnology & Oceanography*, *57*(2), 554–566. https://doi.org/10.4319/lo.2012.57.2.0554

Emerson, S. (2014). Annual net community production and the biological carbon flux in the ocean. *Global Biogeochemical Cycles*, *28*(1), 14–28. https://doi.org/10.1002/2013gb004680

Fawcett, S. E., Lomas, M. W., Casey, J. R., Ward, B. B., & Sigman, D. M. (2011). Assimilation of upwelled nitrate by small eukaryotes in the Sargasso Sea. *Nature Geoscience*, *4*(10), 717–722. https://doi.org/10.1038/ngeo1265

Flombaum, P., Gallegos, J. L., Gordillo, R. A., Rincón, J., Zabala, L. L., Jiao, N., et al. (2013). Present and future global distributions of the marine Cyanobacteria *Prochlorococcus* and *Synechococcus*. *Proceedings of the National Academy of Sciences of the United States of America*, *110*(24), 9824–9829. https://doi.org/10.1073/pnas.1307701110

Flombaum, P., Wang, W. L., Primeau, F. W., & Martiny, A. C. (2020). Global picophytoplankton niche partitioning predicts overall positive response to ocean warming. *Nature Geoscience*, *13*(2), 116–120. https://doi.org/10.1038/s41561-019-0524-2

Flynn, K. J., Skibinski, D. O., & Lindemann, C. (2018). Effects of growth rate, cell size, motion, and elemental stoichiometry on nutrient transport kinetics. *PLoS Computational Biology*, *14*(4), e1006118. https://doi.org/10.1371/journal.pcbi.1006118

Friedlingstein, P., Cox, P., Betts, R., Bopp, L., von Bloh, W., Brovkin, V., et al. (2006). Climate–carbon cycle feedback analysis: Results from the C4MIP model intercomparison. *Journal of Climate*, *19*(14), 3337–3353. https://doi.org/10.1175/jcli3800.1

Galbraith, E. D., & Martiny, A. C. (2015). A simple nutrient-dependence mechanism for predicting the stoichiometry of marine ecosystems. *Proceedings of the National Academy of Sciences of the United States of America*, *112*(27), 8199–8204. https://doi.org/10.1073/pnas.1423917112

Garcia, H. E., Locarnini, R. A., Boyer, T. P., Antonov, J. I., Baranova, O. K., Zweng, M. M., et al. (2013). In S. Levitus, & A. Mishonov Technical (Eds.), *World Ocean Atlas 2013, volume 4: Dissolved inorganic nutrients (phosphate, nitrate, silicate)* [Dataset], NOAA Atlas NESDIS 76, 25 pp. https://doi.org/10.7289/V5F769GT

Garcia, N. S., Fu, F., Sedwick, P. N., & Hutchins, D. A. (2015). Iron deficiency increases growth and nitrogen-fixation rates of phosphorus-deficient marine cyanobacteria. *The ISME Journal*, *9*(1), 238–245. https://doi.org/10.1038/ismej.2014.104

Geider, R. J., & La Roche, J. (2002). Redfield revisited: Variability of C [ratio] N [ratio] P in marine microalgae and its biochemical basis. *European Journal of Phycology*, *37*(1), 1–17. https://doi.org/10.1017/s0967026201003456

Getzlaff, J., & Dietze, H. (2013). Effects of increased isopycnal diffusivity mimicking the unresolved equatorial intermediate current system in an earth system climate model. *Geophysical Research Letters*, *40*(10), 2166–2170. https://doi.org/10.1002/grl.50419

Glover, H. E., Prézelin, B. B., Campbell, L., Wyman, M., & Garside, C. (1988). A nitrate-dependent *Synechococcus* bloom in surface Sargasso Sea water. *Nature*, *331*(6152), 161–163. https://doi.org/10.1038/331161a0

Hein, M., Pedersen, M. F., & Sand-Jensen, K. (1995). Size-dependent nitrogen uptake in micro-and macroalgae. *Marine Ecology Progress Series. Oldendorf*, *118*(1), 247–253. https://doi.org/10.3354/meps118247

Henson, S. A., Sanders, R., Madsen, E., Morris, P. J., Le Moigne, F., & Quartly, G. D. (2011). A reduced estimate of the strength of the ocean's biological carbon pump. *Geophysical Research Letters*, *38*(4), L04606. https://doi.org/10.1029/2011gl046735

Hutchins, D. A., Fu, F. X., Zhang, Y., Warner, M. E., Feng, Y., Portune, K., et al. (2007). CO_2 control of *Trichodesmium* N_2 fixation, photosynthesis, growth rates, and elemental ratios: Implications for past, present, and future ocean biogeochemistry. *Limnology & Oceanography*, *52*(4), 1293–1304. https://doi.org/10.4319/lo.2007.52.4.1293

Hutchins, D. A., Hare, C. E., Weaver, R. S., Zhang, Y., Firme, G. F., DiTullio, G. R., et al. (2002). Phytoplankton iron limitation in the Humboldt Current and Peru Upwelling. *Limnology & Oceanography*, *47*(4), 997–1011. https://doi.org/10.4319/lo.2002.47.4.0997

Ilyina, T., Six, K. D., Segschneider, J., Maier-Reimer, E., Li, H., & Núñez-Riboni, I. (2013). Global ocean biogeochemistry model HAMOCC: Model architecture and performance as component of the MPI-Earth system model in different CMIP5 experimental realizations. *Journal of Advances in Modeling Earth Systems*, *5*(2), 287–315. https://doi.org/10.1029/2012ms000178

Jenkins, W. J., & Doney, S. C. (2003). The subtropical nutrient spiral. *Global Biogeochemical Cycles*, *17*(4). https://doi.org/10.1029/2003gb002085

Juranek, L. W., White, A. E., Dugenne, M., Henderikx Freitas, F., Dutkiewicz, S., Ribalet, F., et al. (2020). The importance of the phytoplankton "middle class" to ocean net community production. *Global Biogeochemical Cycles*, *34*(12), e2020GB006702. https://doi.org/10.1029/2020gb006702

Karl, D. M., Björkman, K. M., Dore, J. E., Fujieki, L., Hebel, D. V., Houlihan, T., et al. (2001). Ecological nitrogen-to-phosphorus stoichiometry at station ALOHA. *Deep Sea Research Part II: Topical Studies in Oceanography*, *48*(8–9), 1529–1566. https://doi.org/10.1016/s0967-0645(00)00152-1

Klausmeier, C. A., Litchman, E., Daufresne, T., & Levin, S. A. (2004). Optimal nitrogen-to-phosphorus stoichiometry of phytoplankton. *Nature*, *429*(6988), 171–174. https://doi.org/10.1038/nature02454

Knapp, A. (2012). The sensitivity of marine N_2 fixation to dissolved inorganic nitrogen. *Frontiers in Microbiology*, *3*, 374. https://doi.org/10.3389/fmicb.2012.00374

Kwiatkowski, L., Aumont, O., Bopp, L., & Ciais, P. (2018). The impact of variable phytoplankton stoichiometry on projections of primary production, food quality, and carbon uptake in the global ocean. *Global Biogeochemical Cycles*, *32*(4), 516–528. https://doi.org/10.1002/2017gb005799

Kwiatkowski, L., Torres, O., Bopp, L., Aumont, O., Chamberlain, M., Christian, J. R., et al. (2020). Twenty-first century ocean warming, acidification, deoxygenation, and upper-ocean nutrient and primary production decline from CMIP6 model projections. *Biogeosciences*, *17*(13), 3439–3470. https://doi.org/10.5194/bg-17-3439-2020

Kwon, E. Y., Sreeush, M. G., Timmermann, A., Karl, D. M., Church, M. J., Lee, S. S., & Yamaguchi, R. (2022). Nutrient uptake plasticity in phytoplankton sustains future ocean net primary production. *Science Advances*, *8*(51), eadd2475. https://doi.org/10.1126/sciadv.add2475

Letscher, R. T. (2023a). PICO simulation of the CESM-BEC (Version v1) [Dataset]. Zenodo. https://doi.org/10.5281/zenodo.8169687

Letscher, R. T. (2023b). PICO source code v1.0: February 24, 2023 Release (Version 1.0). [Software]. Zenodo. https://zenodo.org/badge/latestdoi/606271192

Letscher, R. T., & Moore, J. K. (2015). Preferential remineralization of dissolved organic phosphorus and non-Redfield DOM dynamics in the global ocean: Impacts on marine productivity, nitrogen fixation, and carbon export. *Global Biogeochemical Cycles*, *29*(3), 325–340. https://doi.org/10.1002/2014gb004904

Letscher, R. T., Moore, J. K., Teng, Y. C., & Primeau, F. (2015). Variable C: N: P stoichiometry of dissolved organic matter cycling in the Community Earth System Model. *Biogeosciences*, *12*(1), 209–221. https://doi.org/10.5194/bg-12-209-2015

Letscher, R. T., Primeau, F., & Moore, J. K. (2016). Nutrient budgets in the subtropical ocean gyres dominated by lateral transport. *Nature Geoscience*, *9*(11), 815–819. https://doi.org/10.1038/ngeo2812

Lomas, M. W., Baer, S. E., Mouginot, C., Terpis, K. X., Lomas, D. A., Altabet, M. A., & Martiny, A. C. (2021). Varying influence of phytoplankton biodiversity and stoichiometric plasticity on bulk particulate stoichiometry across ocean basins. *Communications Earth & Environment*, *2*(1), 1–10. https://doi.org/10.1038/s43247-021-00212-9

Lomas, M. W., Bates, N. R., Johnson, R. J., Steinberg, D. K., & Tanioka, T. (2022). Adaptive carbon export response to warming in the Sargasso Sea. *Nature Communications*, *13*(1), 1211. https://doi.org/10.1038/s41467-022-28842-3

Lomas, M. W., Bonachela, J. A., Levin, S. A., & Martiny, A. C. (2014). Impact of ocean phytoplankton diversity on phosphate uptake. *Proceedings of the National Academy of Sciences of the United States of America*, *111*(49), 17540–17545. https://doi.org/10.1073/pnas.1420760111

Lomas, M. W., Bronk, D. A., & van den Engh, G. (2011). Use of flow cytometry to measure biogeochemical rates and processes in the ocean. *Annual Review of Marine Science*, *3*(1), 537–566. https://doi.org/10.1146/annurev-marine-120709-142834

Lomas, M. W., & Moran, S. B. (2011). Evidence for aggregation and export of cyanobacteria and nano-eukaryotes from the Sargasso Sea euphotic zone. *Biogeosciences*, *8*(1), 203–216. https://doi.org/10.5194/bg-8-203-2011

Long, M. C., Moore, J. K., Lindsay, K., Levy, M., Doney, S. C., Luo, J. Y., et al. (2021). Simulations with the marine biogeochemistry library (MARBL). *Journal of Advances in Modeling Earth Systems*, *13*(12), e2021MS002647. https://doi.org/10.1029/2021ms002647

Martiny, A. C., Hagstrom, G. I., DeVries, T., Letscher, R. T., Britten, G. L., Garcia, C. A., et al. (2022). Marine phytoplankton resilience may moderate oligotrophic ecosystem responses and biogeochemical feedbacks to climate change. *Limnology & Oceanography*, *67*(S1), S378–S389. https://doi.org/10.1002/lno.12029

Martiny, A. C., Kathuria, S., & Berube, P. M. (2009). Widespread metabolic potential for nitrite and nitrate assimilation among Prochlorococcus ecotypes. *Proceedings of the National Academy of Sciences of the United States of America*, *106*(26), 10787–10792. https://doi.org/10.1073/pnas.0902532106

Martiny, A. C., Pham, C. T., Primeau, F. W., Vrugt, J. A., Moore, J. K., Levin, S. A., & Lomas, M. W. (2013a). Strong latitudinal patterns in the elemental ratios of marine plankton and organic matter. *Nature Geoscience*, *6*(4), 279–283. https://doi.org/10.1038/ngeo1757

Martiny, A. C., Vrugt, J. A., & Lomas, M. W. (2014). Concentrations and ratios of particulate organic carbon, nitrogen, and phosphorus in the global ocean. *Scientific Data*, *1*(1), 1–7. https://doi.org/10.1038/sdata.2014.48

Martiny, A. C., Vrugt, J. A., Primeau, F. W., & Lomas, M. W. (2013b). Regional variation in the particulate organic carbon to nitrogen ratio in the surface ocean. *Global Biogeochemical Cycles*, *27*(3), 723–731. https://doi.org/10.1002/gbc.20061

Matsumoto, K., Tanioka, T., & Rickaby, R. (2020). Linkages between dynamic phytoplankton C: N: P and the ocean carbon cycle under climate change. *Oceanography*, *33*(2), 44–52. https://doi.org/10.5670/oceanog.2020.203

Moloney, C. L., & Field, J. G. (1989). General allometric equations for rates of nutrient uptake, ingestion, and respiration in plankton organisms. *Limnology & Oceanography*, *34*(7), 1290–1299. https://doi.org/10.4319/lo.1989.34.7.1290

Moore, J. K., Doney, S. C., & Lindsay, K. (2004). Upper ocean ecosystem dynamics and iron cycling in a global three-dimensional model. *Global Biogeochemical Cycles*, *18*(4). https://doi.org/10.1029/2004gb002220

Moore, J. K., Fu, W., Primeau, F., Britten, G. L., Lindsay, K., Long, M., et al. (2018). Sustained climate warming drives declining marine biological productivity. *Science*, *359*(6380), 1139–1143. https://doi.org/10.1126/science.aao6379

Moore, J. K., Lindsay, K., Doney, S. C., Long, M. C., & Misumi, K. (2013). Marine ecosystem dynamics and biogeochemical cycling in the Community Earth System Model [CESM1 (BGC)]: Comparison of the 1990s with the 2090s under the RCP4. 5 and RCP8. 5 scenarios. *Journal of Climate*, *26*(23), 9291–9312. https://doi.org/10.1175/jcli-d-12-00566.1

Moore, L. R., Rocap, G., & Chisholm, S. W. (1998). Physiology and molecular phylogeny of coexisting Prochlorococcus ecotypes. *Nature*, *393*(6684), 464–467. https://doi.org/10.1038/30965

NASA Goddard Space Flight Center, Ocean Ecology Laboratory, Ocean Biology Processing Group. (2018). Sea-Viewing wide field-of-view sensor (SeaWiFS) ocean color data. Retrieved from https://oceandata.sci.gsfc.nasa.gov/cgi/getfile/S19972472010334.L3b_CU_CHL.nc

Nelson, D. M., & Brzezinski, M. A. (1997). Diatom growth and productivity in an oligo-trophic midocean gyre: A 3-yr record from the Sargasso Sea near Bermuda. *Limnology & Oceanography*, *42*(3), 473–486. https://doi.org/10.4319/lo.1997.42.3.0473

Nelson, D. M., Tréguer, P., Brzezinski, M. A., Leynaert, A., & Quéguiner, B. (1995). Production and dissolution of biogenic silica in the ocean: Revised global estimates, comparison with regional data and relationship to biogenic sedimentation. *Global Biogeochemical Cycles*, *9*(3), 359–372. https://doi.org/10.1029/95gb01070

Orchard, E. D., Ammerman, J. W., Lomas, M. W., & Dyhrman, S. T. (2010). Dissolved inorganic and organic phosphorus uptake in *Trichodesmium* and the microbial community: The importance of phosphorus ester in the Sargasso Sea. *Limnology & Oceanography*, *55*(3), 1390–1399. https://doi.org/10.4319/lo.2010.55.3.1390

Oschlies, A. (2002). Nutrient supply to the surface waters of the North Atlantic: A model study. *Journal of Geophysical Research*, *107*(C5), 14-1–14-13. https://doi.org/10.1029/2000jc000275

Palter, J. B., Marinov, I., Sarmiento, J. L., & Gruber, N. (2013). *Large-scale, persistent nutrient fronts of the World Ocean: Impacts on biogeochemistry in chemical oceanography of frontal zones* (pp. 1–38). Springer.

Partensky, F., Blanchot, J., & Vaulot, D. (1999). *Differential distribution and ecology of Prochlorococcus* and *Synechococcus* in oceanic waters: A review (pp. 457–476). Bulletin-Institut Oceanographique Monaco-Numero Special-.

Pasulka, A. L., Landry, M. R., Taniguchi, D. A., Taylor, A. G., & Church, M. J. (2013). Temporal dynamics of phytoplankton and heterotrophic protists at station ALOHA. *Deep Sea Research Part II: Topical Studies in Oceanography*, *93*, 44–57. https://doi.org/10.1016/j.dsr2.2013.01.007

Quéré, C. L., Harrison, S. P., Colin Prentice, I., Buitenhuis, E. T., Aumont, O., Bopp, L., et al. (2005). Ecosystem dynamics based on plankton functional types for global ocean biogeochemistry models. *Global Change Biology*, *11*(11), 2016–2040. https://doi.org/10.1111/j.1365-2486.2005.1004.x

Quigg, A., Finkel, Z. V., Irwin, A. J., Rosenthal, Y., Ho, T. Y., Reinfelder, J. R., et al. (2003). The evolutionary inheritance of elemental stoichiometry in marine phytoplankton. *Nature*, *425*(6955), 291–294. https://doi.org/10.1038/nature01953

Redfield, A. C. (1934). *On the proportions of organic derivatives in sea water and their relation to the composition of plankton* (Vol. 1). University Press of Liverpool.

Redfield, A. C. (1958). The biological control of chemical factors in the environment. *American Scientist*, *46*(3), 230A–221A.

Rhee, G. Y. (1978). Effects of N: P atomic ratios and nitrate limitation on algal growth, cell composition, and nitrate uptake. *Limnology & Oceanography*, *23*(1), 10–25. https://doi.org/10.4319/lo.1978.23.1.0010

Richardson, T. L. (2019). Mechanisms and pathways of small-phytoplankton export from the surface ocean. *Annual Review of Marine Science*, *11*(1), 57–74. https://doi.org/10.1146/annurev-marine-121916-063627

Richardson, T. L., & Jackson, G. A. (2007). Small phytoplankton and carbon export from the surface ocean. *Science*, *315*(5813), 838–840. https://doi.org/10.1126/science.1133471

Séférian, R., Berthet, S., Yool, A., Palmieri, J., Bopp, L., Tagliabue, A., et al. (2020). Tracking improvement in simulated marine biogeochemistry between CMIP5 and CMIP6. *Current Climate Change Reports*, *6*(3), 95–119. https://doi.org/10.1007/s40641-020-00160-0

Sharoni, S., & Halevy, I. (2020). Nutrient ratios in marine particulate organic matter are predicted by the population structure of well-adapted phytoplankton. *Science Advances*, *6*(29), eaaw9371. https://doi.org/10.1126/sciadv.aaw9371

Shire, D. M., & Kustka, A. B. (2015). Luxury uptake, iron storage and ferritin abundance in *Prochlorococcus marinus* (Synechococcales) strain MED4. *Phycologia*, *54*(4), 398–406. https://doi.org/10.2216/14-109.1

Siegel, D. A., Buesseler, K. O., Doney, S. C., Sailley, S. F., Behrenfeld, M. J., & Boyd, P. W. (2014). Global assessment of ocean carbon export by combining satellite observations and food-web models. *Global Biogeochemical Cycles*, *28*(3), 181–196. https://doi.org/10.1002/2013gb004743

Silsbe, G. M., Behrenfeld, M. J., Halsey, K. H., Milligan, A. J., & Westberry, T. K. (2016). The CAFE model: A net production model for global ocean phytoplankton. *Global Biogeochemical Cycles*, *30*(12), 1756–1777. https://doi.org/10.1002/2016gb005521

Smith, R., Jones, P., Briegleb, B., Bryan, F., Danabasoglu, G., Dennis, J., et al. (2010). The parallel ocean program (POP) reference manual: Ocean component of the community climate system model (CCSM) and community earth system model (CESM). Report LAUR-01853. *141*, 1–140.

Sohm, J. A., Ahlgren, N. A., Thomson, Z. J., Williams, C., Moffett, J. W., Saito, M. A., et al. (2016). Co-occurring Synechococcus ecotypes occupy four major oceanic regimes defined by temperature, macronutrients and iron. *The ISME Journal*, *10*(2), 333–345. https://doi.org/10.1038/ismej.2015.115

Sohm, J. A., & Capone, D. G. (2006). Phosphorus dynamics of the tropical and subtropical north Atlantic: Trichodesmium spp. versus bulk plankton. *Marine Ecology Progress Series*, *317*, 21–28. https://doi.org/10.3354/meps317021

Stawiarski, B., Buitenhuis, E. T., & Fallens, M. (2018). The physiological response of seven strains of picophytoplankton to light, and its representation in a dynamic photosynthesis model. *Limnology & Oceanography*, *63*(S1), S367–S380. https://doi.org/10.1002/lno.10745

Stukel, M., Coles, V., Brooks, M., & Hood, R. (2014). Top-down, bottom-up and physical controls on diatom-diazotroph assemblage growth in the Amazon River plume. *Biogeosciences*, *11*(12), 3259–3278. https://doi.org/10.5194/bg-11-3259-2014

Stukel, M. R., Décima, M., Selph, K. E., Taniguchi, D. A., & Landry, M. R. (2013). The role of Synechococcus in vertical flux in the Costa Rica upwelling dome. *Progress in Oceanography*, *112*, 49–59. https://doi.org/10.1016/j.pocean.2013.04.003

Stukel, M. R., & Landry, M. R. (2010). Contribution of picophytoplankton to carbon export in the equatorial Pacific: A reassessment of food web flux inferences from inverse models. *Limnology & Oceanography*, *55*(6), 2669–2685. https://doi.org/10.4319/lo.2010.55.6.2669

Tagliabue, A., Mtshali, T., Aumont, O., Bowie, A. R., Klunder, M. B., Roychoudhury, A. N., & Swart, S. (2012). A global compilation of dissolved iron measurements: Focus on distributions and processes in the Southern Ocean. *Biogeosciences*, *9*(6), 2333–2349. https://doi.org/10.5194/bg-9-2333-2012

Tanioka, T., Garcia, C. A., Larkin, A. A., Garcia, N. S., Fagan, A. J., & Martiny, A. C. (2022). Global patterns and predictors of C: N: P in marine ecosystems. *Communications Earth & Environment*, *3*(1), 271. https://doi.org/10.1038/s43247-022-00603-6

Tanioka, T., & Matsumoto, K. (2017). Buffering of ocean export production by flexible elemental stoichiometry of particulate organic matter. *Global Biogeochemical Cycles*, *31*(10), 1528–1542. https://doi.org/10.1002/2017gb005670

Tanioka, T., & Matsumoto, K. (2020). A meta-analysis on environmental drivers of marine phytoplankton C: N: P. *Biogeosciences*, *17*(11), 2939–2954. https://doi.org/10.5194/bg-17-2939-2020

Teng, Y. C., Primeau, F. W., Moore, J. K., Lomas, M. W., & Martiny, A. C. (2014). Global-scale variations of the ratios of carbon to phosphorus in exported marine organic matter. *Nature Geoscience*, *7*(12), 895–898. https://doi.org/10.1038/ngeo2303

Timmermans, K. R., Van der Wagt, B., Veldhuis, M. J. W., Maatman, A., & De Baar, H. J. W. (2005). Physiological responses of three species of marine pico-phytoplankton to ammonium, phosphate, iron and light limitation. *Journal of Sea Research*, *53*(1–2), 109–120. https://doi.org/10.1016/j.seares.2004.05.003

Torres-Valdés, S., Roussenov, V. M., Sanders, R., Reynolds, S., Pan, X., Mather, R., et al. (2009). Distribution of dissolved organic nutrients and their effect on export production over the Atlantic Ocean. *Global Biogeochemical Cycles*, *23*(4). https://doi.org/10.1029/2008gb003389

Uitz, J., Claustre, H., Gentili, B., & Stramski, D. (2010). Phytoplankton class-specific primary production in the world's oceans: Seasonal and interannual variability from satellite observations. *Global Biogeochemical Cycles*, *24*(3). https://doi.org/10.1029/2009gb003680

Van Mooy, B. A., Fredricks, H. F., Pedler, B. E., Dyhrman, S. T., Karl, D. M., Koblížek, M., et al. (2009). Phytoplankton in the ocean use non-phosphorus lipids in response to phosphorus scarcity. *Nature*, *458*(7234), 69–72. https://doi.org/10.1038/nature07659

Vaulot, D., Gall, F. L., Marie, D., Guillou, L., & Partensky, F. (2004). The Roscoff Culture Collection (RCC): A collection dedicated to marine picoplankton. *Nova Hedwigia*, *79*(1–2), 49–70. https://doi.org/10.1127/0029-5035/2004/0079-0049

Wang, W. L., Moore, J. K., Martiny, A. C., & Primeau, F. W. (2019). Convergent estimates of marine nitrogen fixation. *Nature*, *566*(7743), 205–211. https://doi.org/10.1038/s41586-019-0911-2

Weber, T. S., & Deutsch, C. (2010). Ocean nutrient ratios governed by plankton biogeography. *Nature*, *467*(7315), 550–554. https://doi.org/10.1038/nature09403

Westberry, T., Behrenfeld, M. J., Siegel, D. A., & Boss, E. (2008). Carbon-based primary productivity modeling with vertically resolved photoacclimation. *Global Biogeochemical Cycles*, *22*(2). https://doi.org/10.1029/2007gb003078

Williams, R. G., & Follows, M. J. (1998). The Ekman transfer of nutrients and maintenance of new production over the North Atlantic. *Deep Sea Research Part I: Oceanographic Research Papers*, *45*(2–3), 461–489. https://doi.org/10.1016/s0967-0637(97)00094-0

Wilson, J. D., Andrews, O., Katavouta, A., de Melo Viríssimo, F., Death, R. M., Adloff, M., et al. (2022). The biological carbon pump in CMIP6 models: 21st century trends and uncertainties. *Proceedings of the National Academy of Sciences of the United States of America*, *119*(29), e2204369119. https://doi.org/10.1073/pnas.2204369119

Wiseman, N. A., Moore, J. K., Twining, B. S., Hamilton, D. S., & Mahowald, N. M. (2023). Acclimation of phytoplankton Fe: C ratios dampens the biogeochemical response to varying atmospheric deposition of soluble iron. *Global Biogeochemical Cycles*, *37*(4), e2022GB007491. https://doi.org/10.1029/2022gb007491

Yamamoto, A., Palter, J. B., Dufour, C. O., Griffies, S. M., Bianchi, D., Claret, M., et al. (2018). Roles of the ocean mesoscale in the horizontal supply of mass, heat, carbon, and nutrients to the northern hemisphere subtropical gyres. *Journal of Geophysical Research: Oceans*, *123*(10), 7016–7036. https://doi.org/10.1029/2018jc013969